Accepted Manuscript

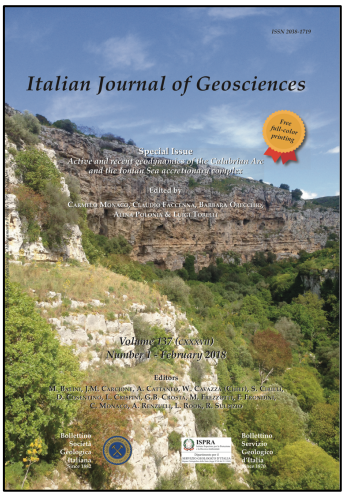

Source areas evolution in the Neogene Agost Basin (Betic Cordillera): implications for regional reconstructions

Manuel Martín-Martín, Francesco Guerrera, Francisco J. Alcalá, Francisco Serrano & Mario Tramontana

To appear in: *Italian Journal of Geosciences*

Received date: 30 November 2017

Accepted date: 10 April 2018

doi: https://doi.org/10.3301/IJG.2018.14

Ital. J. Geosci., Vol. 137 (2018), pp. 00, 0 Figs., 0 tabs. (https://doi.org/10.3301/IJG.2018.14)

Source areas evolution in the Neogene Agost Basin (Betic Cordillera): implications for regional reconstructions

Manuel Martín-Martín (1), Francesco Guerrera (2), Francisco J. Alcalá (1) (3), Francisco Serrano (4) & Mario Tramontana (5)

ABSTRACT

Sedimentary and mineralogical analyses were performed in the Neogene Agost Basin (External Domain, Betic Cordillera) to reconstruct relationships between tectonics and sedimentation, and source areas evolution over time. The sedimentary analysis allowed defining two sedimentary sequences: (1) Lower Stratigraphic Unit, Serravallian *p.p.* and (2) Upper Stratigraphic Unit, post Lower Tortonian (Upper Miocene *p.p.)* separated by an angular unconformity. They consist of marine (lithofacies *L-1* to *L-3*) and continental (lithofacies *L-5* to *L-8*) deposits respectively. The analysis of mineralogical assemblages and some XRD parameters of the sedimentary sequences and older formations allowed recognizing a sedimentary evolution controlled by the activation of different source areas over time. In particular, the Ill+Kln±Sme+Chl clay-mineral association characterizes the supply from Triassic formations; the Ill+Kln+Sme association from Albian formations; the Sme+Ill±Kln+(I-S) and Sme+Ill±Kln associations from Upper Cretaceous *p.p.* formations; and the Sme+Ill±Kln+(I-S) association from Paleogene formations, testifying a tectonic mobility of the basin margins differentiated over time. This reconstruction leads to propose detailed relationships between types of deposits and provenance and not a classic "unroofing", as follows: (i) the lithofacies *L*-1 (lithofacies *L*-2 and *L*-3 were not analysed) is characterized by the Ill+Kln+Sme mineralogical association indicating an origin from the Albian formations; (ii) the lithofacies *L*-4 shows a mixture of Ill+Kln+Sme and Sme+Ill+Kln associations sourced from the Albian and Upper Cretaceous formations; (iii) the lithofacies *L*-5 is characterized by the Sme+Ill±Kln+(I-S) association indicating a provenance from the Upper Cretaceous and Paleogene formations; (iv) the lithofacies *L*-6 to *L*-8 are characterized by the Ill+Kln±Sme+Chl association indicating a supply mainly from Triassic deposits. The evolutionary sedimentary model reconstructed for the Agost Basin, which improves a previous contribution about the same area, has been correlated with those reported in other intramontane Neogene basins in the Betic-Rifian Arc studied with similar resolution, so obtaining useful information for regional reconstructions.

Key words: *Clay-mineral assemblages, Source areas, Tectono-sedimentary evolution, Neogene strike-slip faulting, Betic Cordillera.*

INTRODUCTION

The Agost Basin (SE of Spain) is located in the External Domain of the Betic Cordillera that together with the Rif Chain constitute the Betic-Rifian Arc representing the westernmost Mediterranean Alpine orogenic belt (Fig. 1A) originated by a Miocene tectonics (Guerrera *et alii*, 1993, 2005; Michard *et alii*, 2002; Di Staso *et alii*, 2009; Handy *et alii*, 2010; Carminati *et alii*, 2012; Guerrera & Martin-Martin, 2014; Perrone *et alii*, 2014). Due to well preserved sedimentary record and previous stratigraphic findings (Martín-Martín *et alii*, 2017) this basin can be considered a local key case useful for large-scale reconstructions. The reconstructed sedimentary model and source areas evolution contributed to better delineate the geodynamic-paleogeographic evolution of the eastern External Betic Zone.

The External Betic Domain was the Mesozoic to Tertiary sedimentary cover (Fig. 1B) of the South margin of the Paleozoic Iberian Massif. This passive Alpine margin started to develop during the Mesozoic rifting of the western Tethys producing deep and shallow pelagic blocks separated by normal faults. The evolution of the resulting faults and blocks controlled the successive Mesozoic sedimentary evolution of the margin.

In the region, a tectonic inversion from extension to compression took place close to the K/T boundary (Guerrera *et alii*, 2006, 2014; Guerrera & Martín-Martín, 2014). The Neogene tectonic evolution of this crustal sector is highly controversial and its evolution is still discussed by the international scientific community (see discussions in Sanz De Galdeano & Vera, 1992; and Vera, 2000). For this reason, new studies about this topic are welcomed to increase knowledges. The most accepted models consider that the Mesozoic previously formed normal faults in many cases evolved during the compressive Miocene deformation as strike-slip faults. Bending of strike-slip faults with respect to the direction of movement determined the lateral divergent (in releasing bends) or convergent (in restraining bends) motion of blocks (Allen & Allen, 2005). Moreover, a strike-slip fault single segment could show a successive behavior from releasing bend to restraining bend, caused by changes of the stress axis orientation over time. In the case of the Betic Cordillera and in particular in the Alicante area a progressive reorientation of the convergence during the Miocene is mostly accepted (Sanz De Galdeano & Buforn, 2005). So, from the Serravallian, the Betic Cordillera experienced a horizontal maximum compression with a rotation of the principal axis of stress from E-W to N-S and the resulting deformation gave rise to a strike-slip fault deformation in the whole

(1) Departamento de Ciencias de la Tierra y Medio Ambiente, University of Alicante, Alicante, Spain.
(2) Ex-Dipartimento di Scienze della Terra, della Vita e dell'Ambiente, Università degli Studi di Urbino, Urbino, Italy.
(3) Instituto de Ciencias Químicas Aplicadas, Facultad de Ingeniería, Universidad Autónoma de Chile, Santiago, Chile.
(4) Departamento de Geología y Ecología, University of Málaga, Málaga, Spain.
(5) Dipartimento di Scienze Pure e Applicate (DiSPeA), Università degli Studi di Urbino "Carlo Bo", Urbino, Italy.
Corresponding author e-mail: manuel.martin.m3@gmail.com.

chain. The development of a net of interconnected intramontane basins characterized the Neogene evolution of the eastern Betic Cordillera (Sanz De Galdeano & Vera, 1992; Sissingh, 2008).

In the study area, the faults of this system generated a subsiding area called the Agost Basin by Martín-Martín *et alii* (2017). Terraced sidewall faults and graben subzones developed in the Agost Basin in the context of a dextral stepover with a dextral movement of blocks. This subsiding area is characterized by a Neogene shallow marine and continental infilling controlled by the evolution of several curvilinear faults involving salt tectonics related to basement Triassic rocks (Martín-Martín *et alii*, 2017).

The aim of this paper is to reconstruct the sedimentary evolution of the Neogene Agost Basin (Betic Cordillera, SE Spain) on the basis of mineralogical data that allows deepening previous structural knowledges (Martín-Martín *et alii*, 2017). The identification of the mineralogical associations present in the pre-Neogene sedimentary succession of the area (cfr. Cycles of Vera, 2000) allowed to recognize the possible source areas activated in different times. The obtained data enabled to reconstruct a detailed tectono-sedimentary model.

The space-time distribution of detrital clay minerals in sedimentary successions may provide additional information on the environmental conditions and lithology of the source areas (Gingele *et alii*, 1998; Bolle & Adatte, 2001; Ruffell *et alii*, 2002; Liu *et alii*, 2008; Dou *et alii,* 2010; Moiroud *et alii*, 2012; Alcalá *et alii*, 2013b), as well as on the influence of tectonics on the sedimentary record (Enu, 1986; Martín-Martín *et alii*, 2001; Jamoussi *et alii*, 2003) regarding the most classical provenance studies based on coarser grained sediments analyses. In the Betic-Rifian external domains, the typical clay-mineral assemblages from Triassic (e.g. Dorronsoro, 1978; Puy, 1979), Jurassic (e.g. Palomo *et alii*, 1985; López-Galindo *et alii*, 1994), Cretaceous (e.g. López-Galindo, 1986; Lopez-Galindo & Oddone, 1990; Plestch, 1997; Moiroud *et alii*, 2012), Paleogene (e.g. Martinez-Ruiz *et alii*, 1992; Bolle & Adatte, 2001; Alcalá *et alii*, 2001; Guerrera *et alii*, 2014), and Neogene (e.g. Alcalá *et alii*, 2013a, 2013b; Maaté *et alii*, 2017) terrains are relatively well known and have been used to identify the source area evolution of sedimentary successions (Alcalá *et alii*, 2013a). These relationships between the stratigraphic record and source areas based on clay-mineral studies can be made when the diagenetic influence on clay mineralogy remains low (Ruffell *et alii*, 2002; Liu *et alii*, 2008; Dou *et alii*, 2010; Alcalá *et alii*, 2001, 2013b).

In brief the results obtained represent an integration of previous knowledges and may constitute a resource for the reconstruction of evolutionary models in similar intramontane Neogene basins. This paper represents a first attempt in this direction comparing the recognized evolution with that of other external sectors of the Betic Cordillera, Rif, Tunisian Tell and northern Apennines. The approach followed can be interesting for further regional studies.

GEOLOGICAL SETTING

From the Middle Miocene, after the accomplishment of the westward displacement of the Internal Zones, in the Betic-Rifian Arc many intramontane basins developed with stratigraphic architecture and geometries controlled by re-arrangements of blocks, usually related to strike-slip faults (Sanz De Galdeano & Vera, 1992; Sissingh, 2008). Contemporaneously to the development of intramontane basins the opening of the Mediterranean Sea occurred to form a back-arc basin after the subduction of the Africa Plate under the Mesomediterranean Microplate (*sensu* Guerrera & Martín-Martín, 2014; *and references therein*). In the External Betic Zone during the Middle-Late Miocene a foredeep area called the North Betic Strait (or Proto-Guadalquivir Foreland Basin) connecting the Atlantic Ocean with the Mediterranean Sea (Sanz De Galdeano & Vera, 1992) developed. In the latest Miocene this connection was interrupted in the eastern sector due to the Africa-Iberia convergence, and the North Betic Strait evolved in the Guadalquivir Basin (marine at first, then fluvial) with an opening only to the Atlantic Ocean (Vera, 2000).

Similarly, in the External Rifian Zones (Morocco) equivalent interconnected basins related to the Zoumi, Gharb-Saiss, and Taza Intramontane Basins developed starting from the Middle Miocene, contemporaneously to the S-SW migration of thrust sheets. Other basins (e.g. the Melilla Basin) developed in relation to the extension on the mainland of faults related to the Mediterranean Sea opening (Sissingh, 2008).

The Betic-Rifian Arc intramontane basins were accomplished during the Middle to Late Miocene, contemporaneously with the NW-SE to N-S Africa-Iberia convergence. These basins were grouped by Sanz De Galdeano & Vera (1992) and Sissingh (2008) into four types according to fault orientations and kinematics: (1) NE-SW to NNE-SSW oriented sinistral strike-slip fault basins as the Lorca and Vera Basins in the Betics, and Taza and Melilla Basins in the Rif, due to the NW-SE extension induced by the arc-normal pull of the E-NE trending slab attached to the subducted Iberian Plate; (2) NW-SE and NNE-SSW oriented normal fault basins as the Granada, Guadix-Baza, Ronda, and Fortuna Basins, in the Betics, and Zoumi, Bouhaddi Graben, and Taounate Basins in the Rif, related to the NE-SW extension with a trend similar to the Alboran Shear Zone; (3) N-S oriented fault basins (usually normal faults) as the Mazarrón Basin in the Betics and North African Flysch Trough in the Rif, due to the E-W extension associated with strike-slip faulting; and (4) E-W oriented fault basins (usually normal faults) as the Almanzora and Huercal-Overa Basins, in the Betic, and Saiss and Gharb Basins in the Rif, related to the N-S extension due to the collapse of continental crust by delamination of the lithosphere.

The Agost Basin is located in the Alicante province in the SE Spain (Fig. 1C). This basin was located in the easternmost part of the North Betic Strait in connection with the Mediterranean Sea. Nowadays the Alicante province is characterized by a network of curvilinear faults (in plan view), bounding amygdaloidal, sigmoidal or rhomboid blocks (Guerrera *et alii*, 2014; Martín-Martín *et alii*, 2017; *among others*). During the Neogene these faults formed a complex net of interconnected subsiding areas (usually intramontane basins) separated by structural highs took place. The structural highs were mainly constituted by Cretaceous-Paleogene rocks and along the fault traces that bound the blocks salty Triassic material crops out. The presence of Triassic rocks and

the scarcity of Jurassic ones are related to a major early Cretaceous extensional phase that laminated the Jurassic deposits (De Ruig, 1992). This phase caused an initial event of salt tectonics involving pinch-outs of Triassic clays and gypsum. Most of the diapiric structures of the region were generated by extensional or transtensional faulting in a second salt tectonic event reaching the surface during the Neogene (De Ruig, 1995). Therefore, in this region structural evolution and salt tectonics processes are strongly linked and recorded by sedimentation. In the considered area (Fig. 1C) the main faults characterizing a central segment of the Novelda-Jijona strike-slip Fault Zone have been selected as a key example for the study of the control of fault activity on sedimentation and the reconstruction both of the sedimentary infilling evolution and the history and variations over time of the source areas.

The Novelda-Jijona Strike-Slip Fault Zone in the Agost Basin area consists of a narrow and deep area oriented roughly N80°E, bounded by the "Sierra del Ventós" tectonic sector (900 m high) southward and the "Sierra del Maigmó" tectonic sector (1,200 m high) northward (Fig. 2). Both these reliefs are separated by a sigmoid to rhomboid shaped depression (about 6 km long and 2 km wide) bounded by the "Maigmó" and "Ventós" Faults. Different segments of these faults show orientations ranging from about N50°E to N 90°-100°E.

The deepest central area can be considered a subsiding area related to strike-slip faults where two tectonic sectors can be recognized: (1) the so called Agost Basin that evolved as a graben zone (550-600 m above the sea-level); and (2) the "Sarganella" Range that evolved as a terraced sidewall fault zone (a relative pushed up zone or flower structure *sensu* Twiss & Moores (2007), located 700-800 m above the sea-level) and affected by a dense net of fractures arranged to form sigmoid shaped blocks (map view). The first sector is filled by Neogene deposits, while the second one is mainly characterized by different faulted blocks marked by the presence of exhumed Triassic material and Cretaceous to Paleogene rhomboid outcrops. The two sectors are separated by the "Barranco Blanco" Fault, a feature partly parallel to the "Ventós" Fault whose strike changes from about N50 to N150 and marked by the presence of Triassic clays and gypsum (Fig. 2; plate I: photos 1 and 2).

The present structure of the Agost Basin corresponds with an open syncline (the "Barranco Blanco" Fold) with a 40° to 60° plunging axis (Fig. 2, cross sections). The oldest sediments of the infilling crops out in the eastern perisyncline closure and near the "Sierra del Ventós", while the youngest ones appear westward near the "Sarganella" Range and unconformably seal the "Ventós" Fault in several points. The basin infilling shows a progressive and syn-sedimentary folding resulting in the Barranco Blanco Fold that shows a westward plunging axis. In this structural context the terrains of the Cycle I *p.p.* (Triassic) show a root constituted by a squeezed "salt wall" with a mushroom geometry at the surface (McDonnell *et alii*, 2009) that affects both the "Sarganella" Range and the Agost Basin.

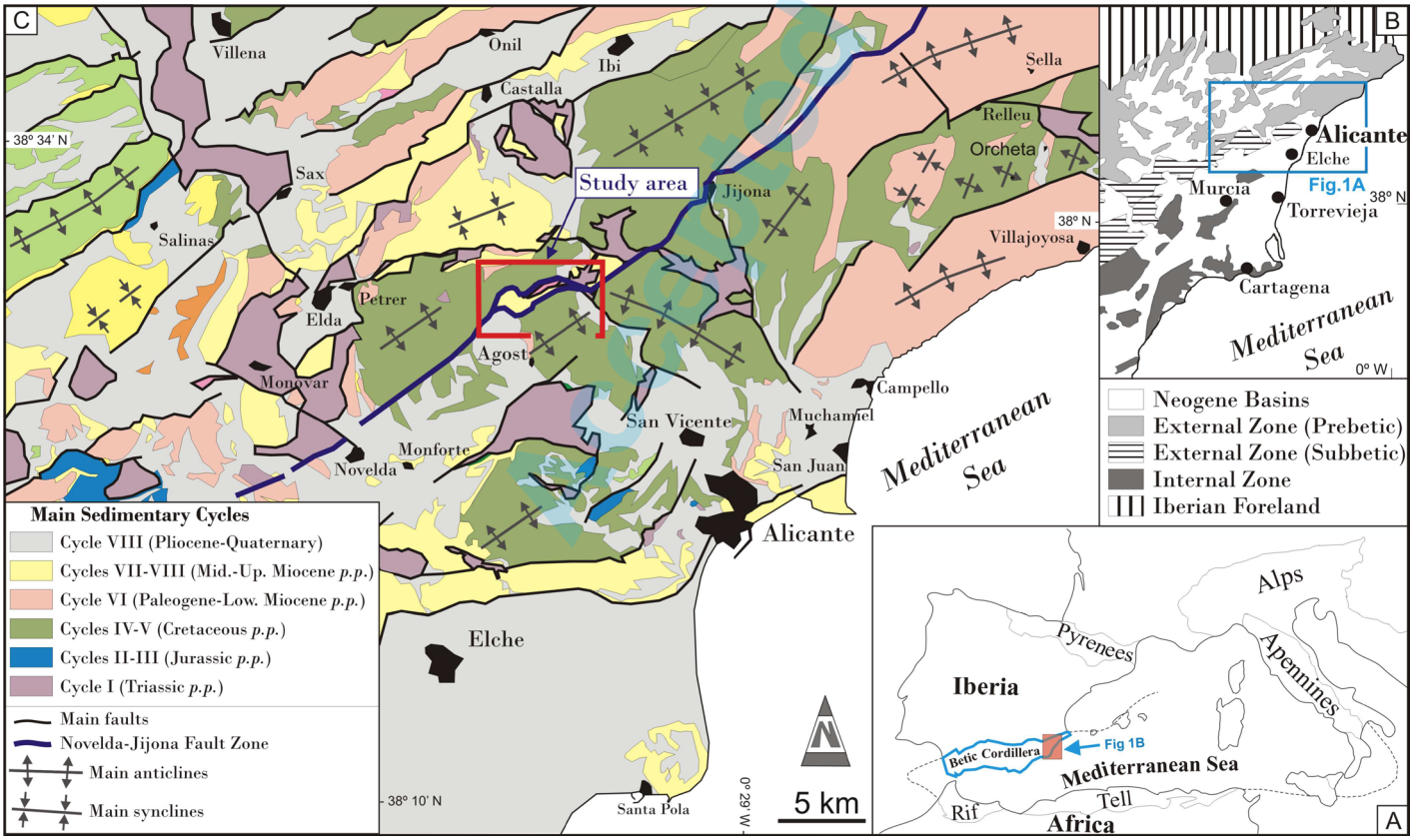

Fig. 1 - A: Index map of the western Mediterranean region with the location of the study area; B: Geological sketch showing the main zones of the eastern Betic Cordillera; C: Geological map based on the main sedimentary cycles proposed by Vera (2000, 2004).

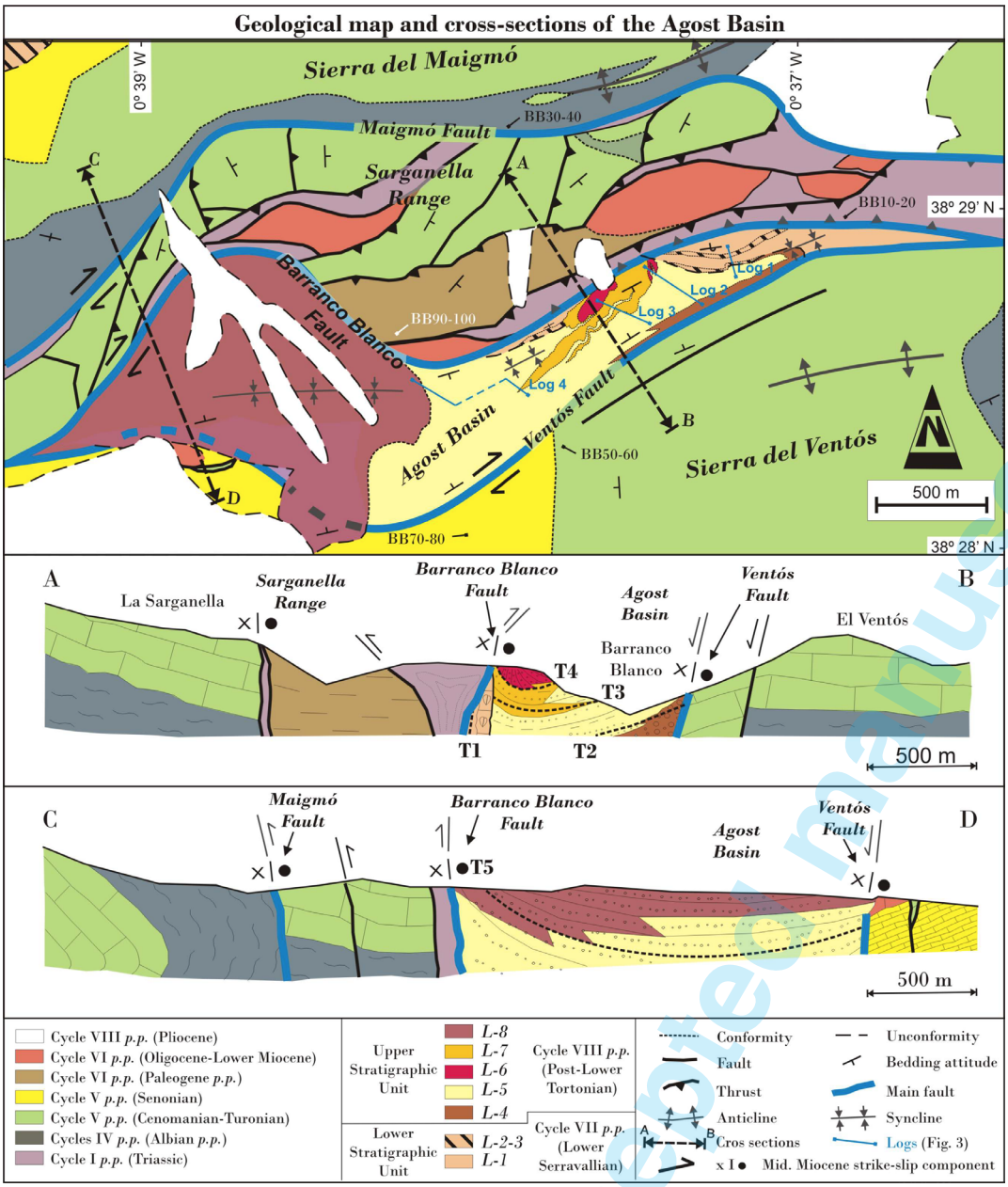

Fig. 2 - Detailed geological map of a sector of the Novelda-Jijona Strike-Slip Fault Zone modified from Martín-Martín *et alii* (2017) including the Agost Basin and surrounding areas (location in Fig. 1C). In the lower part two geological cross-sections of the Agost Basin are shown where the five isochronous lines T1-T5 are also reported. BB identifies code and location of samples for mineralogical analyses, as in tabs. 1 and 2.

MATERIALS AND METHODS

For the purpose of the work, the following field and laboratory analyses were performed: (i) sedimentary analysis in four representative and correlated Neogene stratigraphic sections of the Agost Basin (for a total of 805 m); (ii) sampling of forty-eight clay-rich samples (location in Fig. 2) in different possible source areas on the flanks of the basin (samples BB10 to BB100) and lithofacies of the Neogene Agost Basin (samples BB110 to BB240); (iii) examination of the whole-rock and <2 μm grain-size fraction (clay fraction hereafter) mineralogy of collected samples by X-ray diffraction (XRD) at the Espinardo Laboratory, University of Murcia, by using a Phillips X'PERT MPD Systempert ® diffractometer with automatic slit, CuKα radiation, and 2 to 6° min^{-1} scanning interval from 2° 2θ to 60° 2θ.

For the non-calcareous clay fraction, four oriented mounts on glass slides per sample were prepared following air-drying, ethylene-glycol and dimethyl-sulfoxide solvation for 24 h, and heating at 550°C for 2h for expandable clay-mineral identification (Croudace & Robinson, 1983; Holtzapffel, 1985; Moore & Reynolds, 1997). The position of the (001) series of basal reflections, and eventually other higher-order reflections at the low-angle diffraction region under the diagnostic treatments, were used to identify the clay-mineral groups: smectite and randomly interstratified illite-smectite (15-17 Å), illite (10 Å), kaolinite/chlorite (7 Å) on the glycolated curve taking the 3.57/3.54 Å peak areas ratio into account (Holtzapffel, 1985; Moore & Reynolds, 1997). The reflections and reflecting powers of Schultz (1964), Biscaye (1965), and Holtzapffel (1985) were used to identify and quantify the mineral phases, respectively. The XPowder ® program [http://www.xpowder.com/] was used for the semi-quantitative estimates of the reflection peak areas. Replicate analyses of a few selected samples gave a

precision of ±3% (2σ). Based upon the XRD technique, the semi-quantitative evaluation of each mineral phase (in weight percent, wt. % normalized to 100%) has an accuracy of ~5%. The intensities ration of characteristic reflections peak areas of quartz, smectite and illite were examined to deduce possible diagenetic influences on the mineral phases (Hunziker, 1986; Righi & Elsass, 1996; Drits *et alii*, 1997). The intensities ratio of the Qtz(001)/Qtz(101) peak areas of quartz (Qtz(001)/Qtz(101) ratio hereafter) in the whole-rock XRD diffractograms is a tentative index to discern authigenic (higher values) from secondary quartz (lower values) in the absence of a volcanic component (Eslinger *et alii*, 1973). These authors proposed Qtz(001)/Qtz(101) ratios below 0.3 for secondary quartz. The intensities ratio of the Sme(003)/Sme(002) peak areas of smectite (Sme(003)/Sme(002) ratio hereafter) from ethylene-glycol solvated clay-fraction XRD diffractograms is useful for differentiating dioctahedral and trioctahedral smectites (Moore & Reynolds, 1997). Increased Fe+MgxAl exchange in the mineral structure due to physical weathering under a low diagenetic influence results in decreased intensity of some reflections, indicated by Sme(003)/Sme(002) ratios below 1 for Fe+Mg-rich smectites. The intensities ratio of the Ill(002)/Ill(001) peak areas of illite (Ill(002)/Ill(001) ratio hereafter) from decomposited air-dried clay-fraction XRD diffractograms is an approximate index of the Al x Mg+Fe exchange in the octahedral sheet as the mineral structure transforms by physical processes (Esquevin, 1969). This author proposed the (001) reflection width as indicator of low diagenetic influence only when the Ill(002)/Ill(001) ratio is below 0.3, which indicates a low Al/(Fe+Mg) ratio.

RESULTS

Lithostratigraphic record of the agost basin

The lithostratigraphic record and sedimentary features of the Agost Basin were reconstructed by means of four representative stratigraphic successions (logs 1-4 of Fig. 3, and plate I; also located in Fig. 2) previously studied by Martín-Martín *et alii* (2017). The succession was subdivided into two main stratigraphic sequences separated by an angular unconformity (plate I: photo 3): (1) Lower Stratigraphic Unit (LSU), Serravallian *p.p.*, consisting of marine deposits; and (2) Upper Stratigraphic Unit (USU), Upper Miocene *p.p.*, characterized by continental (lacustrine and fluvial) deposits.

The overlying sub-horizontal Pliocene deposits seal the deformed USU and all previous tectonic structures by a major angular unconformity (plate I: photo 6). The LSU is preserved only in a restricted area of the basin where it shows a thickness of about 100 m. Outside of the Agost Basin this unit was also recognized in the Maigmó Relief (Fig. 2), where it shows the shallowest lithofacies with conglomerates and marly levels. This unit was defined as Tap facies by Vera (2004) in surrounding areas where marls prevail. The LSU is made up of three lithofacies (plate I: photos 1, 2, and 3): *L-1,* whitish marls and marly limestones (44 m thick) rich in foraminifers and spicules of sponges; *L-2*, calcarenitic beds with conglomerate intercalations (5-10 m thick) rich in benthic foraminifera and several kinds of mollusks; *L-3,* calcarenitic beds (50 m thick) rich in large foraminifera, echinoderms, corals, briozoes, ostreids, and brachiopods. This succession indicates a relative sea-level fall, evidenced by a regressive evolution from open to shallow water and restricted marine conditions. This local reconstruction corresponds to the evolutionary trend recognized at the regional scale (Vera, 2004; Guerrera *et alii*, 2006; Guerrera & Martín-Martín, 2014), which is related to a progressive shallowing of the environment towards the northern Prebetic sub-Domain and the consequent deepening to the W-SW, where several structural highs and deep areas occur.

The most extensive and preserved USU (more than 490 m thick) is made up of five lithofacies. The lower part the lithofacies *L-4* is composed of more than 250 m thick of conglomerates, arenites, and whitish clays and silts showing a typical onlap arrangement (plate I: photo 5). Furthermore, considering also grain size of clasts, bad rounding, and position at the base of the reliefs, this unit may indicate a continental foot-cliff depositional environment. The *L-4* is also common in the surrounding area of the Sierra del Ventós relief and sometimes seals the Ventós Fault so representing also a useful marker level for tectonic reconstructions. The lithofacies *L-5*, more than 50 m thick, is made of whitish clays and silts with local black levels (lignite), arenites, and channelized conglomeratic intercalations (plate I: photos 4, 5, and 6). The coarse detritic supply of the channelized conglomerates diminishes northwards (from conglomeratic to siltitic beds); furthermore, the presence of abundant lignite may be also interpreted as indicative of fluvial and lacustrine realms.

The lithofacies *L-6*, more than 90 m thick, is mainly characterized by reddish conglomerates (plate I: photos 3 and 5 to 8) containing blocks of Triassic gypsum (plate I: photo 8) and with a fan shape and arrangement of beds (plate I: photo 7). The conglomeratic beds decrease southwards showing lateral variations to siltstones. In particular, two conglomeratic bodies crop out in the northern side of the Agost Basin (i.e. the Barranco Blanco Fault Zone; Figs. 2 and 3). The lithofacies *L-6* has been interpreted as a progradational deposition of alluvial fan in a fluvial to lacustrine realm.

The lithofacies *L-7* consists of pinkish clays and silts with occasional arenites and conglomeratic intercalations deposited in the northern margin of the basin, arranged in a great depositional body (> 45 m thick) and encompassing the lithofacies *L-6* in the central area of the basin (plate I: photos 3, 5, and 6). The conglomeratic beds of the lithofacies *L-7* decrease southward with the occurrence of lateral variations from conglomerates to siltstones.

The conglomerates of the lithofacies *L-8* (more than 55 m thick), composed of Cretaceous-Paleogene calcareous clasts and Triassic bi-pyramidal quartz and gypsum with a matrix made up of Triassic reddish pelites, shows a progradation and decrease of grain size southward. This lithofacies is arranged in a fan structure sealing the Ventós Fault (Fig. 2) and is fed by the Sarganella Range according to the distribution of coarse deposits and the sense of progradation.

In conclusion, the USU indicates a depositional system consisting of fluvial and lacustrine realms in the central area of the basin, and alluvial fans and cliff deposits in the margins.

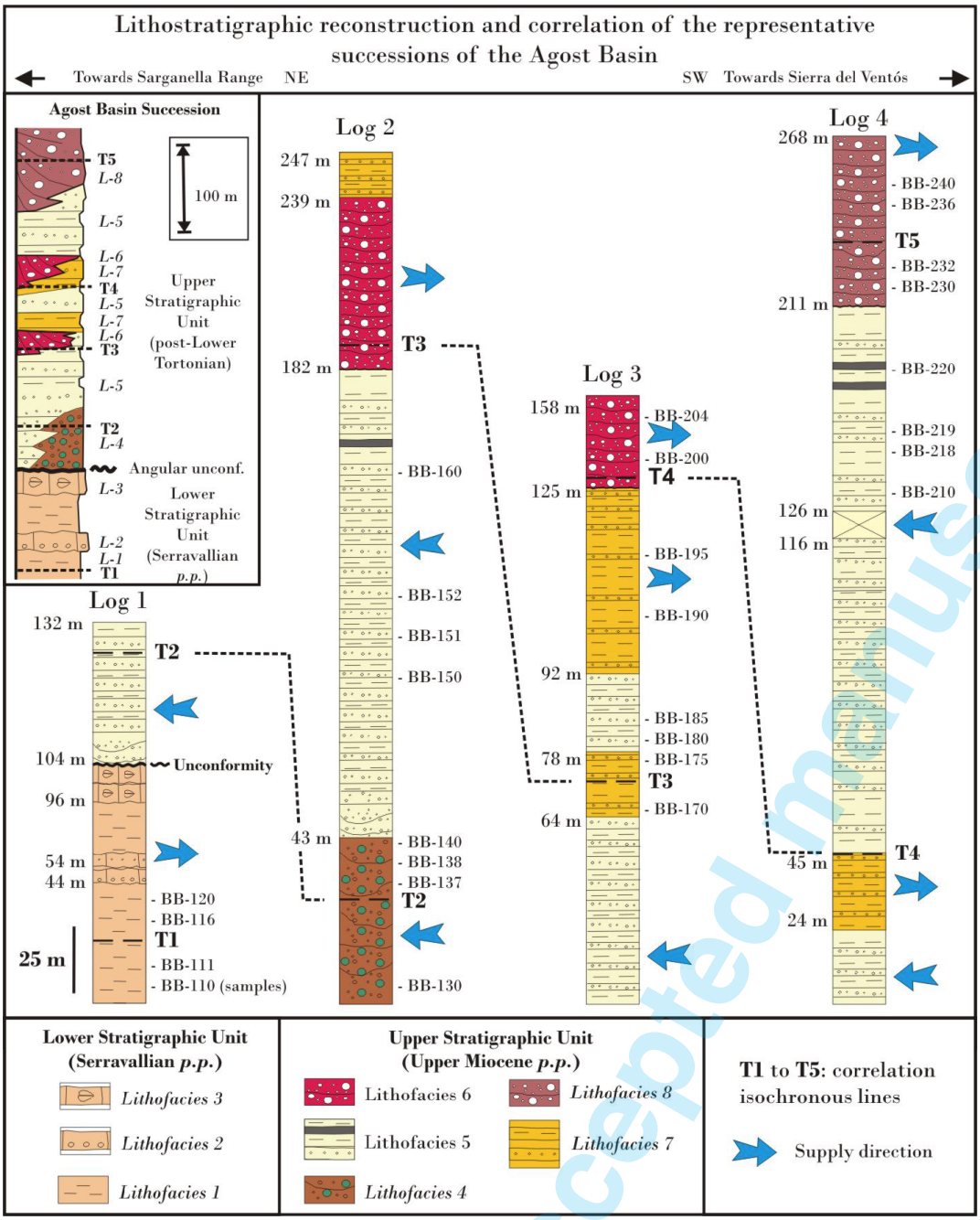

Fig. 3 - Lithostratigraphic record and correlations of four representative successions (logs 1 to 4) of the Agost Basin (location in Fig. 2). The two main sequences (Lower Stratigraphic Unit, LSU and Upper Stratigraphic Unit, USU) separated by an angular unconformity are evidenced. Depositional environments, supplies and the isochronous lines T1-T5 are also indicated.

Mineralogy of the pre-Neogene formations

In the perspective to identify the possible source areas (Sierra del Maigmó, Sarganella Range, and Sierra del Ventós) feeding the Agost Basin in different times, mineralogical associations and XRD parameters of the pre-Neogene formations characterizing all these source areas were studied. For this purpose the samples BB10 to BB100 (located in Fig. 2) collected from the outcropping sedimentary cycles indicated as follows: I (Triassic), IV (Albian *p.p.*), V (Upper Cretaceous *p.p.*), and VI (Paleogene) were examined (Tab. 1; Fig. 4).

Clays, and gypsy clays and pelites lithologies from the Triassic Cycle I include (in wt. % hereafter) phyllosilicates (9-39%), K-feldspar (14-24%), gypsum (5-53%), quartz (5-18%), and minor amounts of plagioclase, magnetite, and hematite. The clay fraction includes illite (67-68%), kaolinite (12-19%), smectite (9-16%), and chlorite (<6%), which characterizes the Ill+Kln±Sme+Chl clay-mineral association. The Qtz(100)/Qtz(101), Sme(003)/Sme(002), and Ill(002)/Ill(001) ratios vary in the 0.21-0.31, 0.72-0.75, and 0.19-0.28 ranges, respectively. Compared to the gypsy clays and pelites, the clays lithology shows: (1) lower amount of gypsum, K-feldspar, and smectite; (2) lower Qtz(100)/Qtz(101) and Ill(002)/Ill(001) ratios; (3) higher amounts of phyllosilicates, quartz, kaolinite, and chlorite; and (4) presence of Fe-oxides (Tab. 1).

Pelites, sandy and silty marls, and marls lithologies from the Albian Cycle IV include calcite (54-66%), dolomite (9-18%), phyllosilicates (14-15%), quartz (7-9%),

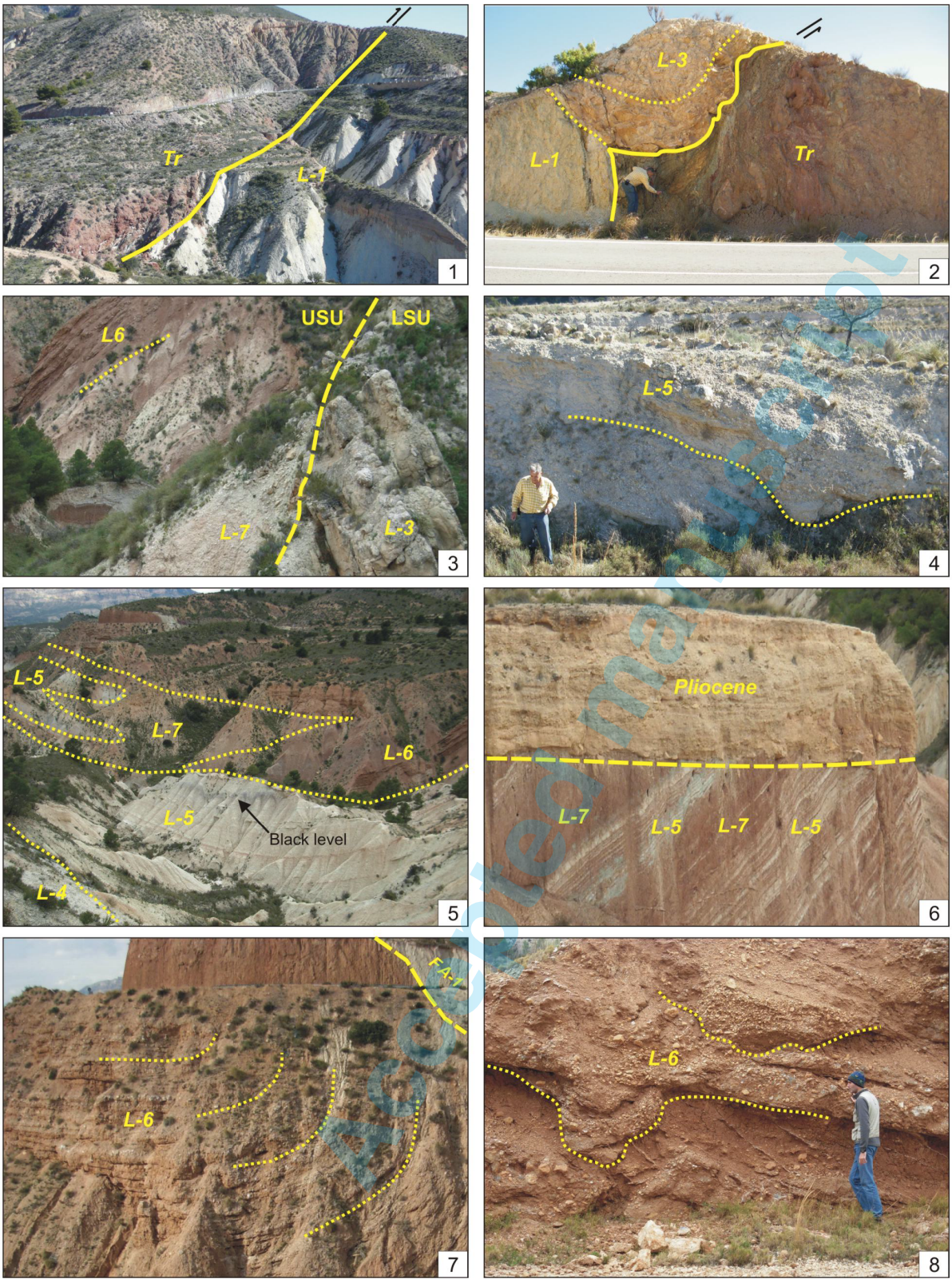

Plate I - Significant outcrops showing tectonic and sedimentary features of deposits of the Agost Basin. 1, mushroom structure constituted by Triassic rocks (Tr) overriding the lithofacies *F-1* (LSU, Lower Serravallian). This structure is also shown in the cross sections of Fig. 2; 2, tectonic contact between the lithofacies *L-1* and *L-3* (USU) and the Triassic salt wall (*Tr*) (see also the geological cross section A-B of Fig. 2); 3, angular unconformity between the LSU (represented by the lithofacies *L-3*) and the USU (represented by the lithofacies *L-6* and *L-7*) (see also the geological cross section A-B of Fig. 2); 4, conglomeratic channelized body of the lithofacies *L-5*; 5, folded USU succession (Barranco Blanco) involving the lithofacies *L-4* and *L-5* and the lateral change of the lithofacies *L-5* to *L-6* and *L-7*; 6, alternating lithofacies *L-5* and *L-7* (USU) topped by the Pliocene deposits by means of an evident angular unconformity; 7, deformed fan deposits of the lithofacies *L-6* (USU) showing a downlap geometry; 8, conglomeratic channelized body of the lithofacies *L-6* (USU) containing gypsum clasts.

TABLE 1

Average whole-rock and <2 µm grain-size fraction mineralogy (in wt. %) of samples from the Sedimentary Cycles I to VI (source areas) (Qtz, quartz; Phy, phyllosilicates; Cal, calcite; Dol, dolomite; Kfs, K-feldspar; Pl, plagioclase; Gp, gypsum; Mag, magnetite; Hem, hematite; Sme, smectite; Ill, illite; Kln, kaolinite; Chl, chlorite; I-S, mixed layer illite-smectite). Intensities ratio of the Qtz(001)/Qtz(101) peak areas of quartz, and Sme(003)/Sme(002) peak areas of smectite and Ill(002)/Ill(001) peak areas of illite under ethylene glycol solvation are included.

Sedimentary				Whole rock									<2 µm grain-size fraction							
Cycle	Age	Sample [a]	Lithology	Qtz	Phy	Cal	Dol	Kfs	Pl	Gp	Mag	Hem	Sme	Ill	Kln	Chl	I-S	Qtz(100)/ Qtz(101)	Sme(003)/ Sme(002)	Ill(002)/ Ill(001)
Cycle VI	Paleogene *p.p.*	BB100	marls	<5	10	89							46	28	24		<5	0.20	0.85	0.26
		BB96	pelitic marls	<5	9	90							45	29	25		<5	0.21	0.86	0.27
		BB95	marls	<5	9	90							43	30	24		<5	0.19	0.85	0.24
		BB90	silty marls	<5	9	90							46	29	23		<5	0.20	0.84	0.25
Cycle V	Senonian *p.p.*	BB80	marly limestones	<5	<5	95							38	30	32			0.30	0.94	0.30
		BB75	marls	<5	<5	96							37	32	31			0.30	0.95	0.34
		BB71	silty marls	<5	<5	96							41	30	29			0.32	0.87	0.29
		BB70	marly limestones	<5	<5	97							41	28	31			0.33	0.86	0.33
	Cenomanian-Turonian *p.p.*	BB60	marly limestones	<5	7	90							61	32	<5		<5	0.27	0.81	0.27
		BB59	silty marls	<5	6	91							63	30	<5		<5	0.28	0.82	0.25
		BB57	marly limestones	<5	6	91							63	29	<5		<5	0.25	0.84	0.26
		BB50	marly limestones	<5	5	92							61	31	<5		<5	0.25	0.85	0.22
Cycle IV	Albian *p.p.*	BB40	pelites	9	15	54	18			5			27	39	34			0.20	0.89	0.16
		BB34	sandy marls	9	14	57	15			5			27	40	33			0.21	0.90	0.19
		BB33	silty marls	7	14	64	10			5			20	45	35			0.20	0.85	0.21
		BB30	marls	7	14	66	9			<5			22	44	34			0.21	0.84	0.18
Cycle I	Triassic *p.p.*	BB20	gypsy pelites	5	10			24	<5	52	7		16	68	12	<5		0.31	0.75	0.28
		BB18	gypsy clays	5	9			23	<5	53	8		16	67	13	<5		0.30	0.74	0.24
		BB12	clays	17	39			14	<5	7	16	6	10	67	19	<5		0.24	0.73	0.21
		BB10	clays	18	39			15	<5	5	17	5	9	67	18	6		0.21	0.72	0.19

[a] Location of samples in fig. 2

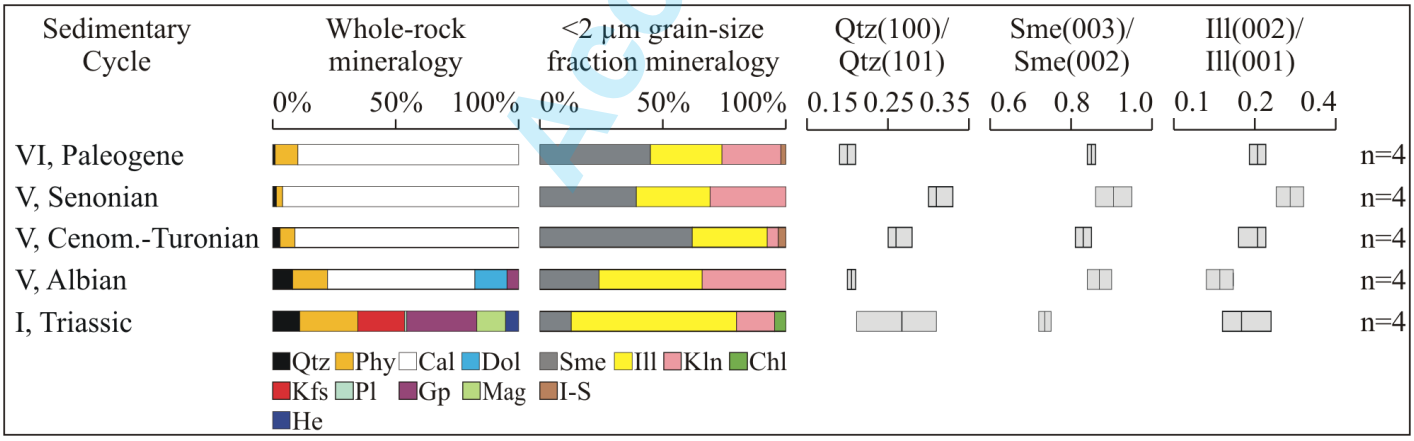

Fig. 4 - Mineralogical results concerning the source areas given as the average value from the set of samples (*n*) in each Sedimentary Cycle included in Tab. 1 for the whole rock and the <2 µm grain-size fraction (in wt. %). Ranges and average values of the intensities ratio of the Qtz(001)/Qtz(101) peak areas of quartz, and Sme(003)/Sme(002) peak areas of smectite and Ill(002)/Ill(001) peak areas of illite under ethylene glycol solvation are included. Acronyms for mineral phases as in Tab. 1.

and gypsum (<5%). The clay fraction includes illite (39-45%), kaolinite (33-35%), and smectite (20-27%), which characterizes the Ill+Kln+Sme clay-mineral association. The Qtz(100)/Qtz(101), Sme(003)/Sme(002), and Ill(002)/Ill(001) ratios vary in the 0.20-0.21, 0.84-0.90, and 0.18-0.21 ranges, respectively. Mineral phases and XRD parameters are quite homogeneous among the analyzed lithologies (Tab. 1).

Marly limestones, silty marls, and marls lithologies both from the Cenomanian-Turonian and Senonian (Cycle V) include calcite (90-97%), phyllosilicates (<7%), and quartz (<5). The clay fraction includes smectite (38-63%), illite (28-32%), kaolinite (<32%), and random mixed layer illite-smectite (I-S hereafter) (<5%). The clay-mineral associations are Sme+Ill±Kln+(I-S) and Sme+Ill+Kln for Cenomanian-Turonian and Senonian, respectively. The Qtz(100)/Qtz(101), Sme(003)/Sme(002), and Ill(002)/Ill(001) ratios vary in the 0.25-0.33, 0.81-0.95, and 0.22-0.34 ranges, respectively. The Cenomanian-Turonian shows differences regarding the Senonian lithologies as: (1) higher amounts of phyllosilicates and smectite; (2) lower amounts of calcite and kaolinite; (3) lower Qtz(100)/Qtz(101), Sme(003)/Sme(002), and Ill(002)/Ill(001) ratios; and (4) presence of random mixed layer I-S (Tab. 1).

Marls, and silty and pelitic marls lithologies from the Paleogene Cycle VI include calcite (89-90%), phyllosilicates (9-10%), and quartz (<5%). The clay fraction includes smectite (43-46%), illite (28-30%), kaolinite (23-25%), and random mixed layer I-S (<5%), which characterizes the Sme+Ill±Kln+(I-S) clay-mineral association. The Qtz(100)/Qtz(101), Sme(003)/Sme(002), and Ill(002)/Ill(001) ratios vary in the 0.19-0.21, 0.84-0.86, and 0.24-0.27 ranges, respectively. Mineral phases and XRD parameters are quite homogeneous among the analyzed lithologies (Tab. 1).

Mineralogy of the Neogene Agost Basin succession

The mineralogical associations and XRD parameters found in the Neogene sedimentary record of the Agost Basin (lithofacies *L*-1 to *L*-8) were examined from samples BB110 to BB240 (Tab. 2; Fig. 5), stratigraphically located in Fig. 3.

The marls lithology in the lithofacies *L*-1 (LSU) includes calcite (62-65%), phyllosilicates (16-18%), quartz (6-11%), K-feldspar (9-10%), and minor amounts of plagioclase. The clay fraction includes illite (37-53%), kaolinite (29-45%), and smectite (18-19%), which characterizes the Ill+Kln+Sme clay-mineral association. The Qtz(100)/Qtz(101), Sme(003)/Sme(002), and Ill(002)/Ill(001) ratios vary in the 0.18-0.28, 0.88-0.89, and 0.15-0.20 ranges, respectively. Mineral phases and XRD parameters are quite homogeneous (Tab. 2).

Silty marls, marls, and pelites lithologies in the lithofacies *L*-4 (USU) include calcite (76-85%), phyllosilicates (9-10%), quartz (6-8%), and minor amounts of dolomite. The clay fraction includes illite (39-56%), smectite (30-31%), and kaolinite (14-30%), which characterizes the Ill+Sme+Kln clay-mineral association. The Qtz(100)/Qtz(101), Sme(003)/Sme(002), and Ill(002)/Ill(001) ratios vary in the 0.15-0.25, 0.79-81, and 0.29-0.30 ranges, respectively. Mineral phases and XRD parameters are quite homogeneous (Tab. 2).

Marls, pelites, and clays lithologies in the lithofacies *L*-5 (USU) include calcite (80-91%), phyllosilicates (5-9%), dolomite (<7%), and quartz (<5%). The clay fraction includes illite (28-52%), smectite (24-40%), kaolinite (11-32%), and minor amounts of random mixed layer I-S, which characterizes the Sme+Ill±Kln+(I-S) clay-mineral association. The Qtz(100)/Qtz(101), Sme(003)/Sme(002), and Ill(002)/Ill(001) ratios vary in the 0.18-0.22, 0.82-0.88, and 0.22-0.29 ranges, respectively. Mineral phases and XRD parameters are quite homogeneous (Tab. 2).

Clays and pelites lithologies in the lithofacies *L*-6 (USU) include dolomite (33-34%), calcite (29-30%), gypsum (17-18), phyllosilicates (11%), and quartz (8-9%). The clay fraction includes illite (48-49%), kaolinite (20%), smectite (13%), and chlorite (18-19%), which characterizes the Ill+Kln±Sme+Chl clay-mineral association. The Qtz(100)/Qtz(101), Sme(003)/Sme(002), and Ill(002)/Ill(001) ratios vary in the 0.24-0.25, 0.79-0.80, and 0.22 ranges,

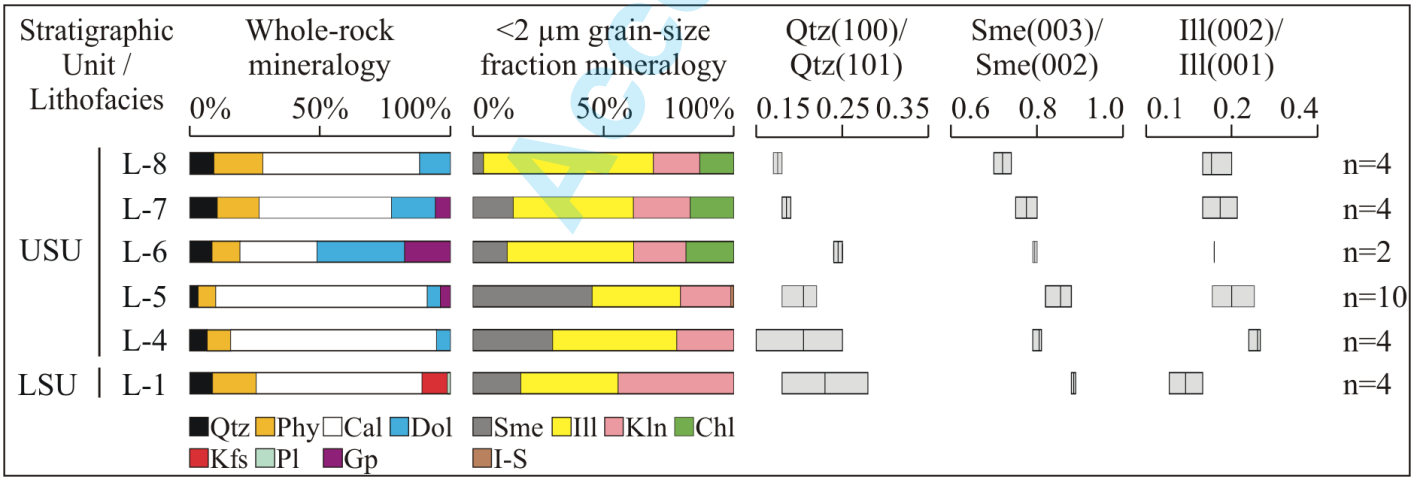

Fig. 5 - Mineralogical results of the Neogene sedimentary record of the Agost Basin (LSU and USU, given as the average value from the set of samples (*n*) in each lithofacies *L-1* to *L-8* included in Tab. 2 for the whole rock and the <2 µm grain-size fraction (in wt. %). Ranges and average values of the intensities ratio of the Qtz(001)/Qtz(101) peak areas of quartz, and Sme(003)/Sme(002) peak areas of smectite and Ill(002)/Ill(001) peak areas of illite under ethylene glycol solvation are included. Acronyms for mineral phases as in Tab. 2.

TABLE 2

Average whole-rock and <2 µm grain-size fraction mineralogy (in wt. %) of samples from the lithofacies *L-1* to *L-8* (Neogene sedimentary record of the Agost Basin) (Qtz, quartz; Phy, phyllosilicates; Cal, calcite; Dol, dolomite; Kfs, K-feldspar; Pl, plagioclase; Gp, gypsum; Sme, smectite; Ill, illite; Kln, kaolinite; Chl, chlorite). Intensities ratio of the Qtz(001)/Qtz(101) peak areas of quartz, and Sme(003)/Sme(002) peak areas of smectite and Ill(002)/Ill(001) peak areas of illite under ethylene glycol solvation are included.

Sedimentary	Lithofacies			Whole rock							<2 µm grain-size fraction							
Stratigraphic Unit	association	Sample [a]	Lithology	Qtz	Phy	Cal	Dol	Kfs	Pl	Gp	Sme	Ill	Kln	Chl	I-S	Qtz(100)/ Qtz(101)	Sme(003)/ Sme(002)	Ill(002)/ Ill(001)
USU	*L-8*	BB240	pelites	7	18	63	12				5	64	17	14		0.18	0.71	0.21
		BB236	silty pelites	9	17	61	13				<5	65	18	14		0.18	0.73	0.20
		BB232	clays	11	20	59	10				<5	65	18	13		0.17	0.70	0.22
		BB230	marls	10	21	57	12				<5	66	18	12		0.17	0.74	0.25
	L-7	BB195	pelites	13	21	35	25			6	13	50	20	17		0.18	0.75	0.20
		BB190	pelites	15	19	35	25			6	14	49	17	20		0.19	0.76	0.22
		BB175	marls	7	12	68	8			5	20	50	30			0.18	0.79	0.26
		BB170	silts	7	13	65	9			6	20	52	28			0.19	0.80	0.24
	L-6	BB204	pelites	8	11	30	33			18	13	48	20	19		0.25	0.80	0.22
		BB200	clays	9	11	29	34			17	13	49	20	18		0.24	0.79	0.22
	L-5	BB220	pelites	<5	8	82	6				50	38	11		<5	0.18	0.85	0.23
		BB219	marls	5	8	81	6				47	38	12		<5	0.18	0.85	0.25
		BB218	pelites	5	8	81	6				45	39	16			0.18	0.85	0.23
		BB210	pelites	<5	9	80	7				46	38	15		<5	0.18	0.86	0.26
		BB185	clays	<5	5	84	<5				30	40	30			0.21	0.82	0.25
		BB180	clays	<5	6	85	<5				28	40	32			0.22	0.82	0.24
		BB160	pelites	<5	6	91					51	24	25			0.22	0.88	0.22
		BB152	pelites	<5	6	90					52	25	23			0.21	0.87	0.25
		BB151	marls	<5	7	90					52	28	20			0.21	0.87	0.29
		BB150	pelites	<5	8	90					50	28	22			0.20	0.88	0.28
	L-4	BB140	pelites	6	9	85					31	39	30			0.25	0.81	0.28
		BB138	silty marls	7	10	83					30	40	30			0.25	0.80	0.30
		BB137	marls	6	8	81	5				31	55	14			0.15	0.79	0.29
		BB130	silty marls	8	10	76	6				30	56	14			0.16	0.81	0.30
LSU	*L-1*	BB120	marls	6	17	65		10	<5		18	53	29			0.18	0.88	0.20
		BB116	marls	8	18	64		9	<5		18	52	30			0.19	0.89	0.19
		BB111	marls	10	16	63		10	<5		19	36	45			0.27	0.89	0.14
		BB110	marls	11	17	62		9	<5		18	37	45			0.28	0.88	0.15

[a] Location of samples in fig. 3

respectively. Mineral phases and XRD parameters are quite homogeneous (Tab. 2).

Marls, silts, and pelites lithologies in the lithofacies *L*-7 (USU) include calcite (35-68%), phyllosilicates (12-21%), dolomite (8-25%), quartz (7-15%), and minor amounts of gypsum. The clay fraction includes illite (49-52%), kaolinite (17-30%), smectite (13-20%), and chlorite (17-20%), which characterizes the Ill+Kln±Sme+Chl clay-mineral association. The Qtz(100)/Qtz(101), Sme(003)/Sme(002), and Ill(002)/Ill(001) ratios vary in the 0.18-0.19, 0.75-0.80, and 0.20-0.26 ranges, respectively. Compared to the marls and silts, the pelites lithology shows: (1) lower calcite, smectite, and kaolinite; (2) lower Sme(003)/Sme(002) and Ill(002)/Ill(001) ratios; (3) higher amount of quartz, phyllosilicates, and dolomite; and (4) presence of chlorite (Tab. 2).

Clays, silty pelites, pelites, and marls lithologies in the lithofacies *L*-8 (USU) include calcite (57-63%), phyllosilicates (17-21%), dolomite (10-13%), and quartz (7-11%). The clay fraction includes illite (64-66%), kaolinite (17-18%), chlorite (12-14%), and minor amounts of smectite, which characterizes the Ill+Kln±Sme+Chl clay-mineral association. The Qtz(100)/Qtz(101), Sme(003)/Sme(002), and Ill(002)/Ill(001) ratios vary in the 0.17-0.18, 0.70-0.74, and 0.20-0.25 ranges, respectively. Mineral phases and XRD parameters are quite homogeneous (Tab. 2).

DISCUSSION

Mineralogical evidences for source areas evolution

Distinctive clay-mineral associations and XRD parameters from sedimentary successions allows

TABLE 3

Clay-minerals associations of the local source areas (Cycles I to VI) and the Neogene sedimentary succession (lithofacies *L-1* to *L-8*). Some clay-mineral associations compiled from the literature for Triassic to Lower Miocene formations in different Subbetic sectors of the Betic Cordillera have been included for comparisons.

Sedimentary Cycles, local source area (this paper)		Clay-mineral association	
Cycle VI, Paleogene		Sme+Ill±Kln+(I-S)	
Cycle V, Senonian (S)		Sme+Ill+Kln	
Cycle V, Cenomanian-Turonian (C-T)		Sme+Ill±Kln+(I-S)	
Cycle IV, Albian		Ill+Kln+Sme	
Cycle I, Triassic		Ill+Kln±Sme+Chl	
Lithofacies, Neogene Agost Basin (this paper)		Clay-mineral association	Main local source area
L6 to L8 (USU)		Ill+Kln±Sme+Chl	Cycle I
L5 (USU)		Sme+Ill±Kln+(I-S)	Cycle V (C-T); Cycle VI
L4 (USU)		Ill+Sme+Kln	Cycle IV; Cycle V (S)
L1 (LSU)		Ill+Kln+Sme	Cycle IV
Regional source areas		Clay-mineral association	Reference
Age	Location [(a)]		
Lower Miocene	(1) Alta Cadena	Sme+Ill+(I-S)±Kln	ALCALÁ *et alii*, (2013a, 2013b)
Lower Miocene	(2) Tajo Almarado	Sme+Ill+(I-S)±Kln	ALCALÁ *et alii*, (2013a, 2013b)
Lower Miocene	(3) Argüelles	Sme+Ill±(I-S)+Kln	ALCALÁ *et alii*, (2013a, 2013b)
Paleogene	(4) Alta Cadena	Sme+Ill±Kln+(I-S)	ALCALÁ *et alii*, (2001)
Paleogene	(5) Tajo Almarado	Sme+Ill±Kln+(I-S)	ALCALÁ *et alii*, (2001)
Paleogene	(6) Alamedilla	Sme+Ill±Kln	BOLLE & ADATTE (2001)
Paleogene	(7) Pila-Carche	Sme+Ill±Kln+(I-S)	GUERRERA *et alii*, (2014)
Paleogene	(8) Agost	Sme+Ill±Kln+(I-S)	MARTINEZ-RUIZ *et alii*, (1992)
Upper Cretaceous	(9) Puerto del Viento	Sme+Ill	LÓPEZ-GALINDO (1986)
Upper Cretaceous	(10) Alamedilla	Sme+Ill±Kln	LÓPEZ-GALINDO (1986)
Upper Cretaceous	(11) Cerrajón	Sme+Ill±Kln	LÓPEZ-GALINDO (1986)
Upper Cretaceous	(12) Guadalupe	Sme+Ill±Kln	LÓPEZ-GALINDO (1986)
Upper Cretaceous	(13) Agost	Sme+Ill+Kln	MARTINEZ-RUIZ *et alii*, (1992)
Lower Cretaceous	(14) Río Argós	Ill+Sme±(I-S)+Kln	MOIROUD *et alii*, (2012)
Lower-Middle Jurassic	(15) Colomera	Ill+Sme±(I-S)+Chl	PALOMO *et alii*, (1985)
Lower-Middle Jurassic	(16) Zegrí	Ill+Sme±(I-S)+Chl+Kln	PALOMO *et alii*, (1985)
Lower Jurassic	(17) La Cerradura	Ill+Sme±Chl	PALOMO *et alii*, (1985)
Triassic	(18) Moraleda	Ill+Chl±Sme+Kln	DORRONSORO (1978)
Triassic	(19) Huelma	Ill+Chl±Sme+Kln	PUY (1979)

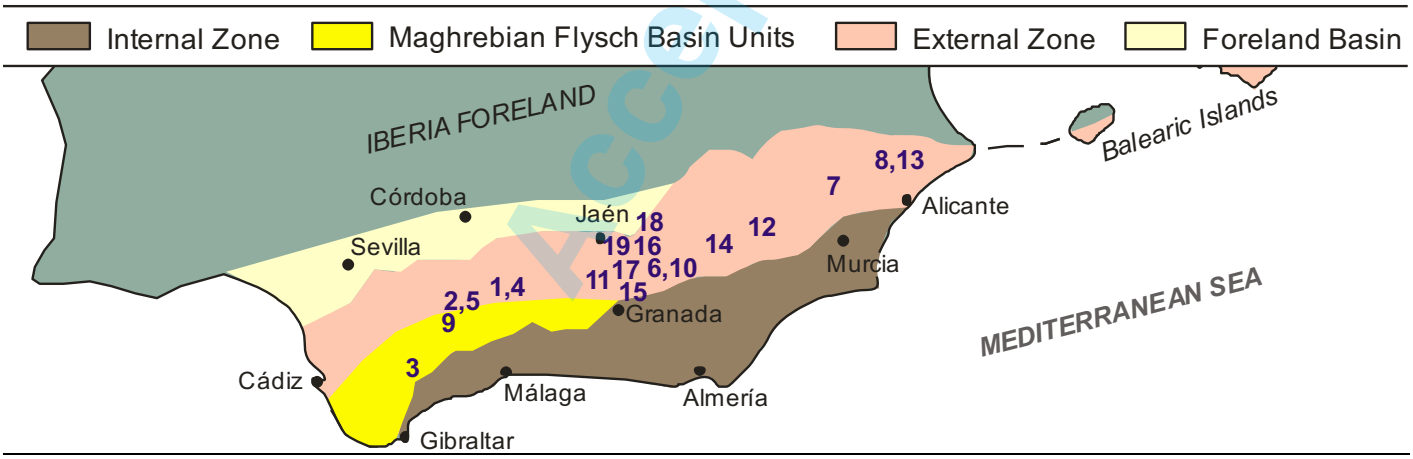

identifying the evolution of supplies from possible sources areas (GINGELE *et alii*, 1998; BOLLE & ADATTE, 2001; RUFFELL *et alii*, 2002; LIU *et alii*, 2008; DOU *et alii*, 2010; MOIROUD *et alii*, 2012; ALCALÁ *et alii*, 2013b), as well as to clarify associated isochrones induced by tectonics (ENU, 1986; MARTÍN-MARTÍN *et alii*, 2001; JAMOUSSI *et alii*, 2003). A low diagenetic overprint is a prerequisite for using the temporal distribution of clay-mineral assemblages (RUFFELL *et alii*,

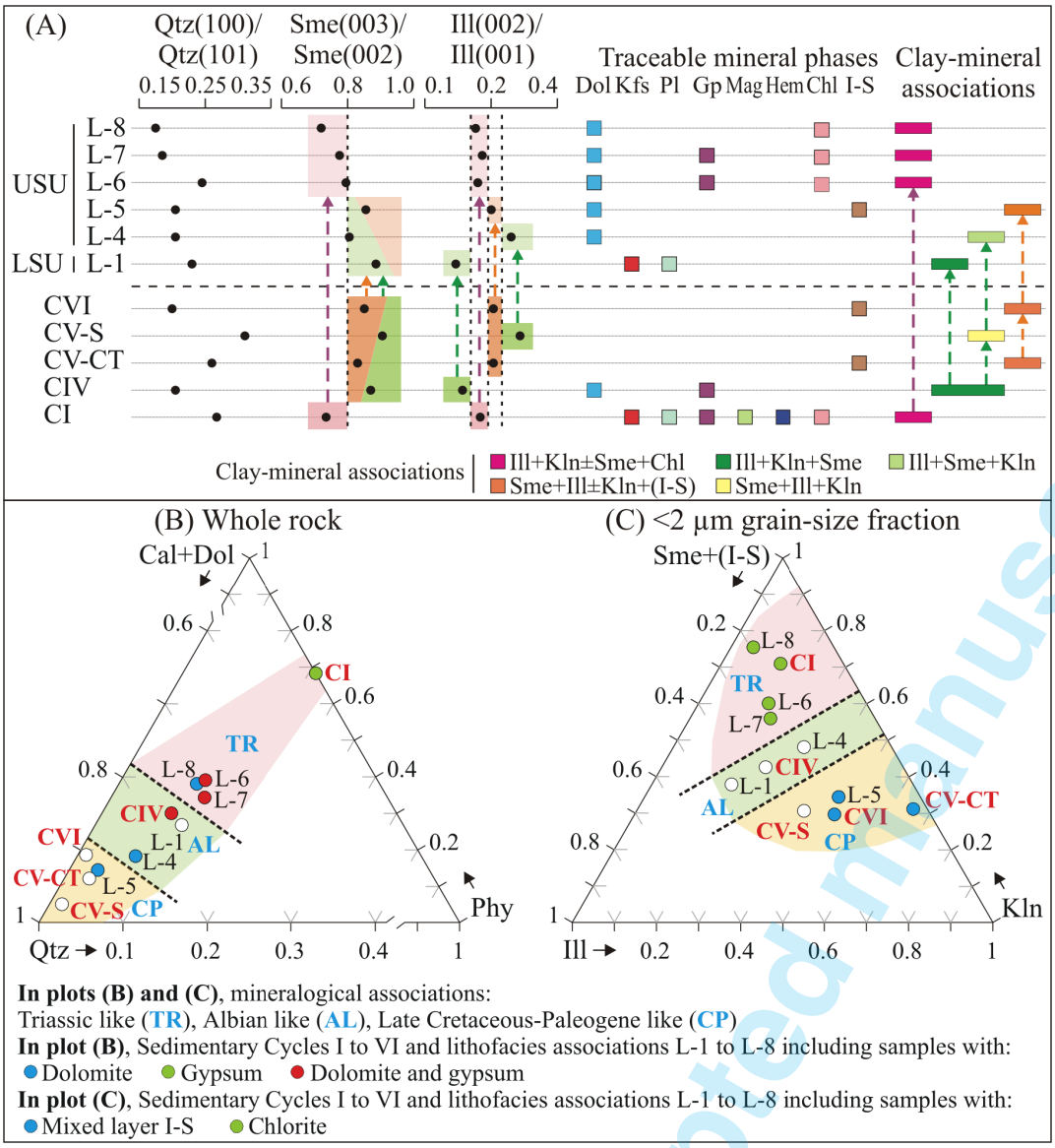

Fig. 6 - (A) Comparative plots of XRD parameters, traceable mineral phases, and clay-mineral associations of the Neogene sedimentary record of the Agost Basin (LSU and USU, including the lithofacies *L-1* to *L-8*) and source areas (Sedimentary Cycles I to VI as Triassic *p.p.*, CI; Albian *p.p.*, CIV; Cenomanian-Turonian *p.p.*, CV-CT; Upper Cretaceous *p.p.*, CV-S; and Paleogene *p.p.*, CVI); purple, green, and orange dotted lines identify supplies from predominant Triassic, Cretaceous, and Upper Cretaceous-Paleogene source areas, respectively. The ternary plots for the whole-rock (B) and the <2 µm grain-size fraction (C) mineralogy, given as the average value (in wt. %) from the set of samples in each Sedimentary Cycle (Tab. 1, Fig. 4) and lithofacies (Tab. 2, Fig. 5), show three compositional fields corresponding to predominant Triassic like (TR), Albian like (AL), and Upper Cretaceous-Paleogene like (CP) mineralogical associations mixing in variable proportions to determine the mineralogical associations from *L-1* to *L-8*. Samples with gypsum and chloride as typical Triassic mineral phases to identify the Triassic influence in *F-1* to *F-8* are indicated. Acronyms for mineral phases as in tabs. 1 and 2.

2002; Liu *et alii*, 2008; Dou *et alii*, 2010; Moiroud *et alii*, 2012; Alcalá *et alii*, 2013b).

In addition, the clay-mineral associations indicating source areas in the Subbetic zone are well-known (Tab. 3): (1) Ill+Kln±Sme+Chl for Triassic formations (Dorronsoro, 1978; PUY, 1979); (2) Ill+Sme±(I-S) with additional variable amounts of Chl±Kln for Jurassic formations (Palomo *et alii*, 1985; López-Galindo *et alii*, 1994); (3) Ill+Sme±(I-S)+Kln for Lower Cretaceous formations (Moiroud *et alii*, 2012); (4) Sme+Ill and Sme+Ill±Kln for Upper Cretaceous formations (López-Galindo, 1986; Martinez-Ruiz *et alii*, 1992; Moiroud *et alii*, 2012); (4) Sme+Ill±Kln+(I-S) and Sme+Ill±Kln for Paleogene formations (Martinez-Ruiz *et alii*, 1992; Alcalá *et alii*, 2001; Bolle & Adatte, 2001; Guerrera *et alii*, 2014); and (5) Sme+Ill±(I-S)+Kln and Sme+Ill±Kln+(I-S) for Lower Miocene formations (Alcalá *et alii*, 2013a, 2013b)

For these purposes, both mineralogical assemblages and XRD parameters of the possible source areas from neighboring Triassic-Paleogene successions (Fig. 4) of the Maigmó Massif, Sarganella Range, and Ventós Massif, and the Neogene Agost Basin succession (Fig. 5) were examined (Fig. 6).

Relative changes in the clay-mineral shape (height and width) peaks on XRD diffractograms have been widely used for tentative evaluations of the exchange or uptake of cations and/or the removal of hydroxide interlayers of inherited clay-mineral phases induced by physical weathering under a low diagenetic influence (Hunziker, 1986; Righi & Elsass, 1996; Drits *et alii*, 1997; Moiroud *et alii*, 2012). The Sme(003)/Sme(002) ratio is useful for differentiating dioctahedral and trioctahedral smectite, as basic criteria to identify the diagenesis degree. This ratio is < 1 in all the studied samples from Cycles I to VI (source areas) and lithofacies *L-1* to *L-8* (Neogene sedimentary successions), thus suggesting a low abundance of Al-rich phases like nontronite and saponite, whose ratios are > 1 (Moore & Reynolds, 1997), indicative of low diagenesis (Drits *et alii*, 1997; Liu *et alii*, 2008). Sme(003)/Sme(002) ratios < 1 in lithofacies *L-1* to *L-5* could indicate the predominance of Mg-rich phases like montmorillonite and beidellite from Cycles IV to VI (Fig. 6A). The

chemical data according to Alcalá *et alii* (2013a) showed the predominance of Mg-rich smectite in other Neogene Betic-Rifian external sectors including inherited clay-mineral assemblages from neighboring Jurassic (e.g. López-Galindo *et alii*, 1994), Cretaceous (e.g. López-Galindo, 1986; Lopez-Galindo & Oddone, 1990; Plestch, 1997; Moiroud *et alii*, 2012), and Paleogene (e.g. Martinez-Ruiz *et alii*, 1992; Bolle & Adatte, 2001; Alcalá *et alii*, 2001) successions. Sme(003)/Sme(002) ratios < 1 in Lithofacies *L*-6 to *L*-8 could nevertheless indicate the predominance of inherited Fe-rich phases from the Triassic Cycle I, whose samples provided similar ratios (Fig. 6A). The Ill(002)/Ill(001) ratio is useful for differentiating the progressive Al x Fe+Mg substitution in the octahedral sheet as the mineral structure transforms by physical weathering in Fe- and Mg-rich media, such as in the study area in particular, and other Betic-Rifian external sectors in general (Alcalá *et alii*, 2013a; Maaté *et alii*, 2017). Al/(Fe+Mg) ratios below 0.3 are documented under weak burial diagenesis (Esquevin, 1969; Hunziker, 1986). Comparable values in the lithofacies *L*-1 and Albian Cycle IV, in the lithofacies *L*-4 and Upper Cretaceous (Senonian) Cycle V, in the lithofacies *L*-5 and Upper Cretaceous (Cenomanian-Turonian) Cycle V and Paleogene Cycle VI, and in the lithofacies *L*-6 to *L*-8 and Triassic Cycle I are observed (Fig. 6A), thus the Ill(002)/Ill(001) ratio being useful to distinguish the source areas that supply each lithofacies over time. The (Qtz(001)/Qtz(101) ratio has not provided clear relationships between source areas and lithofacies, although a decreasing general trend from *L*-1 to *L*-8 is observed, perhaps due to secondary reworking processes (Fig. 6A).

The presence (and sometimes absence) of some clay-mineral phases in sedimentary successions provides additional criteria to qualify the diagenetic influence and identify the source area evolution. For instance the smectite, which has been found in all Cycles and lithofacies, is quite sensitive to temperature rise with burial depth, and tends to disappear above 200°C, after an exponential rate of illitisation between 120°C and 150°C giving transient abundances of mixed-layer I-S (Nadeau & Bain, 1986; Lanson *et alii*, 2009), as described by Moiroud *et alii* (2012) in other Subbetic sectors. However, random mixed layer I-S has always been identified in traces in some samples from Cycles V and VI, and Lithofacies L-5. There is not compositional information about mixed layer I-S in this sector, although variable abundances of smectite sheets in R0 mixed layers I/S can be assumed from the 15-17 Å range explored and data reported by Alcalá *et alii* (2001, 2013a) in other Subbetic sectors, thus indicating weak burial diagenesis at most. Despite clays, marls, pelites, and silts lithologies from lithofacies *L*-6 to *L*-8 are illite- and chlorite-rich, no mixed-layer chlorite-smectite has been identified. The presence of this mineral phase could indicate a diagenetic influence, as reported by Deconinck (1987) in Cretaceous marly sediments in southern France.

The presence of traceable dolomite, K-feldspar, plagioclase, gypsum, Fe-oxides, chlorite, and mixed layer I-S in Cycles I to VI can help to identify a given source area (Fig. 6A). However, the origin of some of these mineral phases may be controversial. For instance, dolomite may come from neo-formation processes in lacustrine realms under certain thermodynamics conditions and abundance of base cations, detrital supplies from a given source area, or by a combination of both processes in variable (usually unknown) proportions. Based on the described lacustrine influence in lithofacies *L*-4 and *L*-5, a combination of neo-formation and minor detrital supplies could have taken place, while a predominant inherited origin is proposed in the continental (alluvial) lithofacies *L*-6 to *L*-8.

Two ternary plots for the main (end-members) whole-rock (Fig. 6B) and clay-fraction (Fig. 6C) mineral phases have been built to show the compositional field of Cycles I to VI and lithofacies *L-1* to *L-8* (LSU and USU). These plots allow interpreting mixtures in varying proportions of mineralogical assemblages from Triassic to Paleogene source areas identified in lithofacies *L-1* to *L-8*, as basic criteria to deduce changes in the supply and erosion of source areas over time.

The Ill+Kln+Sme clay-mineral association identified in the Albian Cycle IV was also found in the lithofacies *L*-1 (LSU) and the beginning of lithofacies *L*-4 (USU) (Figs. 6A and 6C). Also, the Sme(003)/Sme(002) and Ill(002)/Ill(001) ratios are quite similar (Fig. 6A). In addition, the presence of K-feldspar and traces of plagioclase in the lithofacies *L*-1 could suggest a minor supply from the Triassic deposits (Fig. 6B). A main supply from the Albian Cycle IV is proposed for lithofacies *L*-1.

The Ill+Sme+Kln clay-mineral association identified in lithofacies *L*-4 (USU) seems to be the result of the variable mixing of clay-mineral associations Ill+Kln+Sme from the Albian Cycle IV and Sme+Ill+Kln from the Senonian Cycle V, respectively (Figs. 6A and 6C). The presence of dolomite (Fig. 6B) could suggest combined processes of neo-formation in lacustrine realms and a minor supply from Albian deposits. The higher Ill(002)/Ill(001) ratios would identify the Senonian supply (Fig. 6A).

A combined supply from the Cenomanian-Turonian Cycle V and the Paleogene Cycle VI is proposed as source areas for the lithofacies *L*-5 (USU), as deduced from the same Sme+Ill±Kln+(I-S) clay-mineral association, where mixed layer I-S is the most distinctive clay-mineral phase (Fig. A and C). Also the main whole-rock mineralogy is quite similar (Fig. 6B). The presence of dolomite in some samples could suggest neo-formation and a minor supply from the Albian deposits (Fig. 6A). The Ill(002)/Ill(001) ratios seem to confirm a preferential supply from Cenomanian-Turonian and Paleogene terrains (Fig. 6A).

The Ill+Kln±Sme+Chl clay-mineral association identified in the Triassic Cycle I is systematically found in lithofacies *L*-6 to *L*-8 (USU), where chlorite is the most distinctive clay-mineral phase (Fig. A and C). The presence of gypsum in lithofacies *L*-6 and *L*-7 corroborates this source. Lithofacies *L*-8 does not contain gypsum (Fig. 6A), thus suggesting a long alluvial transport that would have caused its dissolution. Reworking of neo-formed dolomite in previous lacustrine realms (lithofacies *L*-4 and *L*-5) may be also considered. The absence of K-feldspar, plagioclase, and Fe-oxides suggests reworking and weathering. These lithofaces show the lower Sme(003)/Sme(002) and Ill(002)/Ill(001) ratios, distinctive of the Triassic Cycle I (Fig. 6A).

The source-area history described suggests a complex erosional evolution. Deposits were initially fed by Albian terrains, later by Late-Upper Cretaceous-Paleogene successions, and finally by Triassic terrains probably with a minor supply from the Neogene sedimentary infilling reworking. This unroofing record relates the timing of tectonics (uplift and subsidence) which determines the areas of the basin to be eroded. So, not a classic

"unroofing" with a linear inverse record in ages of terrains eroded (from youngest to oldest) is evidenced. In the following section the mapping of sedimentary bodies is combined with the stratigraphic data to explain better this reconstruction.

Tectono-sedimentary evolution

The strike-slip faults affecting the Agost Basin were studied by Martín-Martín *et alii* (2017) proposing a geodynamic evolution characterized by several stages (see below). Contemporaneously to this evolution a depositional regressive trend has been evidenced because marine sediments of the LSU are followed by lacustrine and alluvial deposits in the USU. This regressive trend is related to regional factors and not to the local tectonics because it is recorded in the entire Betic Cordillera and Rif (Vera, 2000; Sissingh, 2008).

From the Middle Miocene the study area was characterized by the presence of faults showing lateral (horizontal) movements (Martín-Martín *et alii*, 2017). The N50 trending "Novelda-Jijona" Fault Zone, the stepover of faults, and the clock-wise bending of Agost Basin segment allowed a dextral transtensile motion of blocks developing the incipient basin as a subsiding graben (a terraced sidewall fault subzone) located between the Sierra del Maigmó and Sierra del Ventós reliefs, and also the "Sarganella" Range as a relative raised area. The closure of the Agost Basin was related to a tectonic inversion due to a N-S oriented main stress occurring close to the Latest Miocene-Pliocene boundary and allowing a pure compressive motion of blocks that caused the deformation and squeeze of the basin (Martín-Martín *et alii*, 2017).

The marine sedimentation of the LSU occurred in the lower Serravallian and the mineralogical data suggest a supply mainly from Albian succession (Tab. 4). According to the field data (Fig. 2) the more reasonable source area is the Sierra del Maigmó where the Albian terrains crops out; see the arrows 1 in the paleogeographic map and the time-line T1 from the paleogeographic cross section in Fig. A. The deposition of the LSU was coeval to the regression recorded by a sedimentation change from marine marls and calcarenites to channeled deltaic conglomerates. This regression favored the erosion and exhumation of reliefs when the strike-slip faulting began to develop (mainly in the Maigmó Fault Zone). A central deepening area became the incipient Agost Basin as a part of a net of intramontane basins (Fig. 7A).

The continental deposition of the Upper Miocene *p.p.* USU started as a consequence of the regression above an unconformity showing a marked erosive surface. The tectono-sedimentary evolution of the USU is modeled in the paleogeographic sketch map and cross-sections of Fig. 7B where four isochronous-lines (T2-T5) are also outlined to follow easily the sediment progression. Changes over time of the mapped coarse clastic bodies coming from opposite areas (lithofacies *L-4* and *L-5* from south and lithofacies *L-6* to *L-8* from north) were probably related to alternating activation of fault zones (Tab. 4).

According to the mineralogical findings during the deposition of the lithofacies *L-4* (USU) Albian but also Upper Cretaceous and probably some Paleogene terrains were eroded (Tab. 4). The position of the deposits of lithofacies *L-4* in the Sierra del Ventós surroundings indicates such sector as a source area due to the activation at that time of the Ventós Fault (see arrow 2 in the paleogeographic map and time-line T2 in the paleogeographic cross section in Fig. 7B). From this period the incipient Agost Basin should probably developed disconnected from the net of intramontane basins with activation of the border faults and the change to continental realms. The following deposits belong to lithofacies *L-5* with mineralogical features indicating erosion of Upper Cretaceous to Paleogene terrains probably also derived from the Sierra del Ventós (Tab. 3). In this lithofacies the presence of resedimented microfossils also gave details concerning the erosive history of the Upper Cretaceous-Paleogene-Neogene successions, including the Langhian-lowest Serravallian stratigraphic interval of the LSU.

Successive alluvial fans developed in the northern margin of the basin, close to the Barranco Blanco Fault. These sedimentary bodies were arranged in a southward downlap and are characterized by deposits that vary laterally (lithofacies *L-6* and *L-7*) close to time-lines T3 and T4 and that were supplied by the Sarganella Range (Fig. 7). These alluvial fans constitute the first clear evidence of a Triassic source area in the northern margin of the basin as corroborated also by the typical Triassic mineralogical association found (Tab. 4). The proposed source area is the Sarganella Range, according to the present outcroppings of Triassic bodies, which should be tectonically active in that moment; see arrows 3-4 in the paleogeographic map and time-lines T3-T4 in the paleogeographic cross section in Fig. 7B. This northern supply produced localized sedimentary bodies that quickly but progressively migrated westward (Fig. 7B).

The end of the deposition in the Agost Basin coincided with a third wide alluvial fan (lithofacies *L-8*; USU). This fan invariably coming from the northwestern margin is characterized by clasts originated from Cretaceous-Paleogene terrains and by Triassic materials from northern sources areas or associated with reworked lithofacies *L-6* and *L-7*, as the mineralogical findings indicated (Tab. 4). This prograding basinward sedimentation was also related to the erosion of the uplifting reliefs of the Sarganella Range where all the above-mentioned terrains crop out; see arrow 5 in the paleogeographic map and time-line T5 in the paleogeographic cross section in Fig. 7B.

The recognition of different supply-areas, located mainly in the northern margin of the Agost Basin, suggested strong tectonic activity of the Barranco Blanco Fault in the upper part of the USU. This activity caused a push-up and the erosion of tectonic blocks in the Sarganella Range, and probably the reworking of the lithofacies *L-6* and *L-7*. Furthermore, this tectonic activity allowed the exhumation of Triassic bodies (mainly clays and gypsum) that reaching the paleo-surface assumed the mushroom shape visible nowadays (Fig. 2; plate I, photos 1 and 2), extending both over the Sarganella Range and the margin of the Agost Basin (Fig. 7B). The rapid erosion caused a quick unroofing and the progradational deposition (lithofacies *L-6* to *L-8*) of a great amount of Triassic clays and gypsum on the northern margin of the basin.

The deposition of the lithofacies *L-8* alluvial fan sealed the Ventós Fault in the western part of the Agost Basin (Fig. 7B), while the Pliocene deposits evidence the end of sedimentation in the basin and the beginning of erosion (Fig. 2; plate I, photo 6).

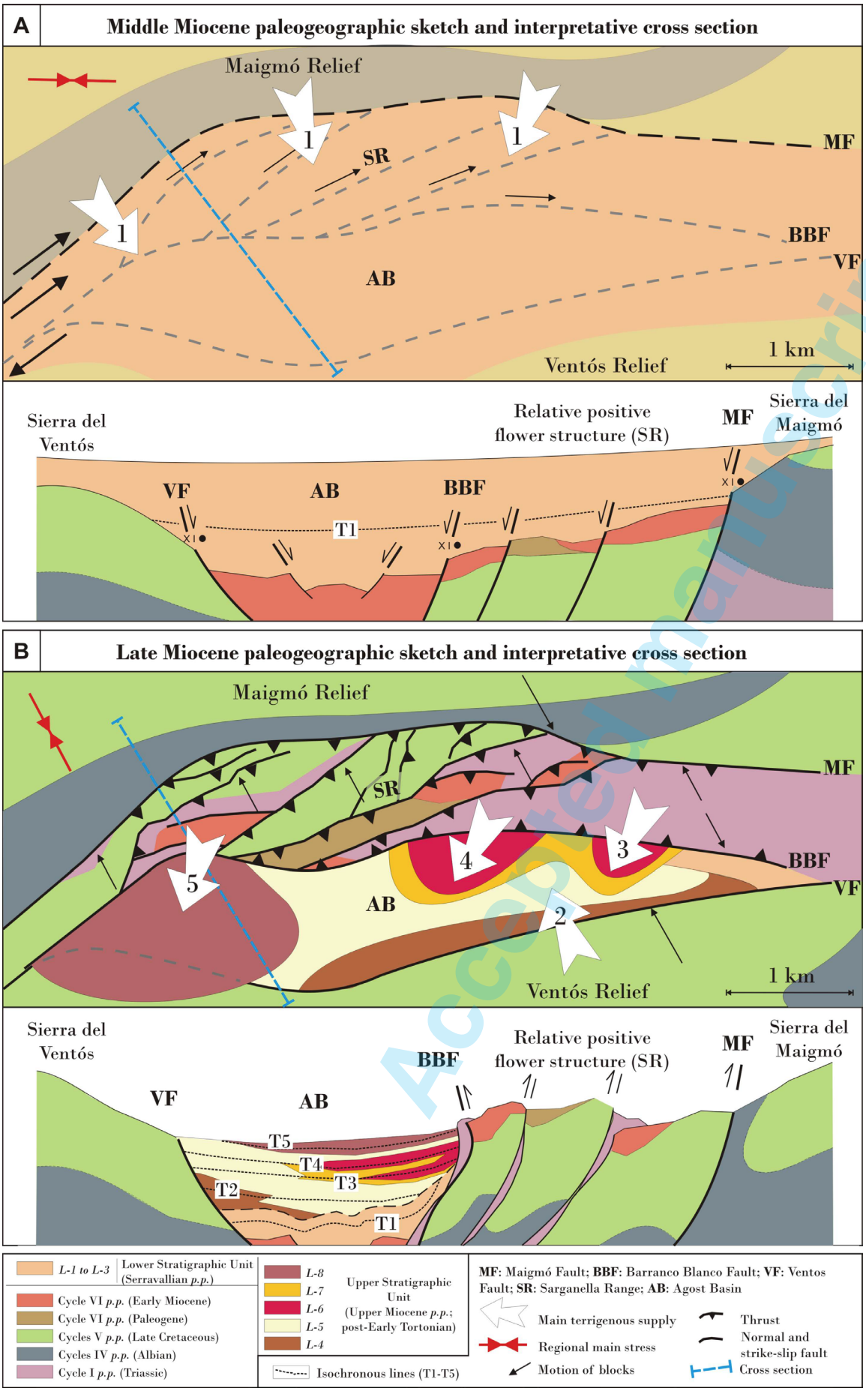

Fig. 7 - Tectono-sedimentary evolutionary model with location of source areas of the Agost Basin and surrounding areas. A: Middle Miocene stage (Lower Stratigraphic Unit); B: Late Miocene stage (Upper Stratigraphic Unit).

TABLE 4

Main sedimentary and mineralogical data, and source areas concerning the infilling of the Agost Basin.

Stratigraphic units (Agost Basin)	Age	Lithofacies	Source areas	Cycles of Vera (2000) eroded in different times	Mineralogical features [a]
Upper Stratigraphic Unit	Upper Miocene *p.p.* (post-Lower Tortonian)	*L-6* to *L-8*	Sarganella Range (northern margin of the basin with migration of supply areas westward)	Cycle I (Diapiric intrusion, Triassic)	Ill+Kln±Sme+Chl Triassic clay-mineral association. Tracers: Gp and Chl. Sme(003)/ Sme(002) ratios <0.75
		L-5	Ventós Massif (southern margin of the basin)	Cycles V and VI (Upper Cretaceous to Paleogene *p.p.*)	Sme+Ill±Kln+(I-S) Upper Cretaceous (Cenomanian-Turonian) and Paleogene clay-mineral association. Tracers: Dol and mixed layer I-S
		L-4		Cycle IV to Cycle VI (Albian *p.p.* to Paleogene *p.p.*)	Ill+Kln+Sme Albian and Sme+Ill+Kln Upper Cretaceous (Senonian) clay-mineral associations. Tracers: Dol. Ill(002)/Ill(001) ratios >0.25
Lower Stratigraphic Unit	Serravallian *p.p.*	*L-1*	Maigmó Massif (northern margin of the basin)	Cycle IV (Albian *p.p.*)	Ill+Kln+Sme Albian clay-mineral association. No tracers. Ill(002)/Ill(001) ratios <0.2

[a] Acronyms for mineral phases as in Tabs. 1 and 2.

Regional paleogeographic considerations

In the External Betic Zone the intramontane basins (Fig. 8) were related to the North Betic Strait (or Proto-Guadalquivir Foreland Basin) connecting during the Middle and the beginning of the Late Miocene the Atlantic Ocean with the Mediterranean Sea (Sanz De Galdeano & Vera, 1992). The Agost Basin was located in the easternmost part of this North Betic Strait in connection with the Mediterranean Sea during Middle Miocene. The Africa-Iberia convergence led to the North Betic Strait closure in the eastern Betics, that would have caused the isolation of the Agost Basin and the sedimentation change from marine to continental.

The Agost Basin, that is related to the Novelda-Jijona strike-slip fault (NE-SW oriented), has a bending reaching an orientation close to E-W (Figs. 1 and 8). This basin could be comprised in the NE-SW oriented strike-slip fault basins of the Betic-Rifian belt but contrary to what has been proposed by Sanz De Galdeano & Vera (1992), the strike slip fault has a dextral kinematics during the Middle Miocene. The E-W orientation of the Agost Basin is a local feature being not correlable with the E-W fault basins since it represents a clear case of strike-slip basin and for its location so far from the Internal Betic Zones is not geometrically compatible with the N-S extension due to collapse by delamination of thickened lithosfere (Vera, 2004). The above reported informations could indicate that although the basins can be grouped according to Sanz De Galdeano & Vera (1992), in detail some basins could be the expression of a more complex paleogeographic-geodynamic evolution.

The general stratigraphic successions of the Betic-Rifian intramontane basins reflect their complex tectonic and depositional history and the relative sea-level changes. A general regressive deposition developed characterized during the Middle Miocene by deep turbiditic to shallow marine platform deposits that evolve during the Late Miocene from shallow marine platform to fan delta deposits, followed by continental lacustrine and fluvial sediments deposited in the Latest Miocene to Quaternary. A similar evolution can be reconstructed also for the Agost Basin. All the Betic-Rifian successions are affected by numerous unconformities and gaps (Sissingh, 2008). A common feature in most of the intramontane basins is the appearing of resedimented Triassic rocks at different stratigraphic levels. These deposits are well documented in the eastern External Betics during the Middle-Late Miocene appearing usually embedded in marly platform sediments and interpreted as olithostrome-like or "salt glacier" deposits (Wenkert, 1979; Tent-Manclús *et alii*, 2000; Estévez *et alii*, 2007; Sissingh, 2008). In the eastern External Zones of the Betic Cordillera the "salt glaciers" are related to overflow of Triassic clayey and salty materials from the basal level of stacked superficial nappes or diapirs, similarly to what interpreted by Martín-Martín *et alii* (2017) for the Agost Basin. Also the study presented in this paper, reflects the existence of such type of Triassic deposits in the Agost Basin, but the approach used allowed to reach further and detailed information concerning the source area in any moment of the sedimentary record. Similar studies are missing in much of the basins mentioned in this section making it impossible to deepen these regional considerations.

FINAL REMARKS

The Agost Basin is a subsiding area related to a NE-SW to E-W oriented strike-slip fault. A dextral transtensile motion of blocks generated a graben structure (a terraced sidewall fault subzone) between the Sierra del Maigmó and the Sierra del Ventós reliefs with the "Sarganella" Range as a relative raised area.

The stratigraphic succession of the Agost Basin is subdivided into two main sequences separated by an

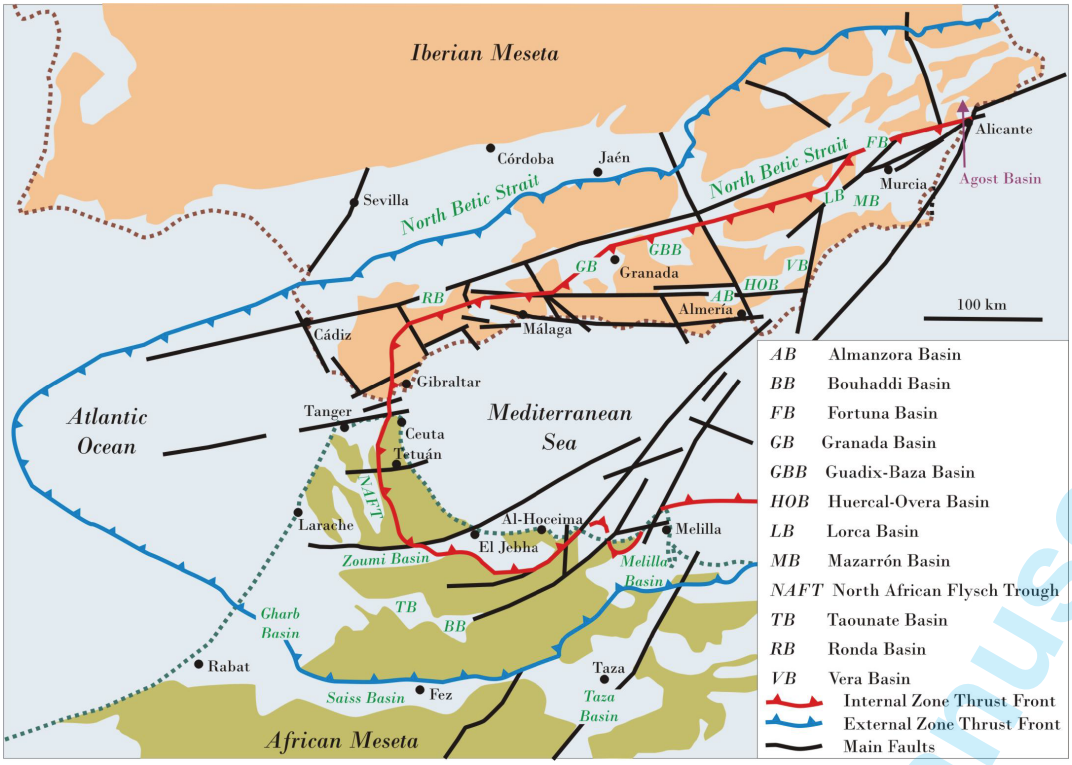

Fig. 8. - Paleogeographic reconstruction showing the Neogene basins of the Betic-Rif chain at the Serravallian-Tortonian boundary (modified from SANZ DE GALDEANO & VERA, 1992; VERA, 2000; SISSINGH, 2008).

angular unconformity: (1) Lower Stratigraphic Unit/LSU (marine deposits, lowest Serravallian), and (2) Upper Stratigraphic Unit/USU (continental lacustrine and fluvial deposits, post-lower Tortonian-pre Pliocene).

The LSU (about 100 m thick) shows a regressive trend from open to restricted marine conditions, within which three lithofacies (*L-1* to *L-3*) rich in benthic foraminifera, echinoderms, corals, briozoes, ostreids, and brachiopod are described. The lithofacies *L*-1 (lithofacies *L*-2 and *L*-3 were not analyzed) is characterized by the Ill+Kln+Sme clay-mineral association probably fed by the Albian succession from the Sierra del Maigmó. The presence of K-feldspar and traces of plagioclase could suggest a minor supply from the northern Triassic deposits.

The more extensive and preserved USU (more than 490 m thick) represents continental realms (fluvial and lacustrine deposits in the depocentral area and alluvial fans and cliff deposits in the margins) depicted by five lithofacies (*L-4* to *L-8*). The changes over time of the coarse clastic bodies coming from opposite areas (lithofacies *L-4* and *L-5* from south and lithofacies *L-6* to *L-8* from north) are probably related to the alternating activation of fault zones. The lithofacies *L-4* consists of a variable mixing of Ill+Kln+Sme and Sme+Ill+Kln clay-mineral associations interpreted as nourished by the erosion of Albian and Upper Cretaceous (Senonian) and minority Paleogene-Miocene terrains. The presence of dolomite and the higher Ill(002)/Ill(001) ratios could corroborate these two main source areas, respectively. The location of the lithofacies *L-4* around the Sierra del Ventós indicates such sector as the source area related to the contemporaneous activation of the Ventós Fault. The Sme+Ill±Kln+(I-S) clay-mineral association of the lithofacies *L-5* suggests a supply derived from the erosion of Upper Cretaceous (Cenomanian-Turonian) to Paleogene terrains from the Sierra del Ventós. The Ill(002)/Ill(001) ratios corroborate these two main source areas. The increasing amount of dolomite upward is probably due to neo-formation processes in lacustrine realms and a minor detrital supply. The more recent alluvial fans developed in the northern margin of the basin close to the Barranco Blanco Fault are the lithofacies *L-6* to *L-8*, characterized by a southward downlap. The Ill+Kln±Sme+Chl clay-mineral association indicates a Triassic source located in the northern margin of the basin. The presence of dolomite, gypsum, and chlorite, as well as the lower Sme(003)/Sme(002) and Ill(002)/Ill(001) ratios, are other distinctive features of the Triassic deposits. The end of the deposition in the Agost Basin corresponds with the third wide alluvial fan (lithofacies *L-8*) coming from the northern margin of the basin and sealing the southern margin of the Ventós fault. The above record of source areas evidences a complex "unroofing" controlled by a complex tectonic activity of uplifting and subsiding blocks alternating in time.

The origin of most of intramontane basins in the Betic-Rifian Chain is related to local extensional processes in the general framework of the NW-SE to N-S Africa-Iberia convergence. The origin and evolution of the Agost Basin was thought to be related to the orientation and bending of the Novelda-Jijona strike-slip fault producing a context of dextral displacement of blocks. This basin could be included in the NE-SW oriented strike-slip fault basins defined by SANZ DE GALDEANO & VERA (1992) but with a different kinematics (i.e. dextral) during the Middle Miocene.

The mineralogical evidences corroborate the usefulness of detrital clay minerals and their XRD parameters for detailed reconstruction of sedimentary evolutions, adding a better resolution to the classical provenance studies based on coarser grained sediments. This study allowed

reconstructing the tectono-sedimentary evolution of a small basin with a good reconstruction of its time/space (vertical and lateral) evolution. So, this basin can be also useful for wide-scale regional reconstructions for instance the Betic-Rifian Arc.

Acknowledgments

Research supported by: Research Project CGL2016-75679-P, Spanish Ministry of Education and Science; Research Groups and Projects of the Generalitat Valenciana, Alicante University (CTMA-IGA); Research Group RNM 146, Junta de Andalucía; Grants from University of Urbino Carlo Bo, responsible M. Tramontana. The revision of a previous version of the manuscript by P. Alfaro is also acknowledged.

REFERENCES

Alcalá F.J., Martín-Martín M. & López-Galindo A. (2001) - *Clay mineralogy of the Tertiary sediments in the Internal Subbetic of Málaga Province (S Spain): implication for geodynamic evolution.* Clay Minerals, **36**, 615-620.

Alcalá F.J., Guerrera F., Martín-Martín M., Raffaelli G. & Serrano F. (2013a) - *Geodynamic implications derived from Numidian-like distal turbidites deposited along the Internal-External Domain Boundary of the Betic Cordillera (S, Spain).* Terra Nova, **25**, 119-129.

Alcalá F.J., López-Galindo A. & Martín-Martín M. (2013b) - *Clay mineralogy as a tool for integrated sequence stratigraphic and palaeogeographic reconstructions: Late Oligocene-Early Aquitanian Western Internal South Iberian Margin, Spain*. Geological Journal, **48**, 363-375.

Allen P.A. & Allen J.R. (2005) - *Basin Analysis: Principles and Applications*. Blackwell, Boston, 549 pp.

Biscaye P.E. (1965) - *Mineralogy and sedimentation of recent deep sea clay in the Atlantic Ocean and adjacent seas and oceans.* Geological Society American Bull., ***76***, 803-832.

Bolle M.P. & Adatte T. (2001) - *Palaeocene-early Eocene climatic evolution in the Tethyan realm: clay mineral evidence*. Clay Minerals **36**, 249-261.

Carminati E., Lustrino M. & Doglioni C. (2012) - *Geodynamic evolution of the central and western Mediterranean: Tectonics vs. igneous petrology constraints*. Tectonophysics, **579**, 173-192.

Croudace J.W. & Robinson N.D. (1983) - *A simple, rapid and precise smear method for the preparation of oriented clay mounts.* Clay Minerals, **18**, 337-340.

Deconinck J.F. (1987) - *Identification de l'origine détritique ou diagénétique des assemblages argileux: le cas des alternances marne-calcaire du Crétacé inférieur subalpin.* Bulletin de la Société Géologique de France, **3**, 139-145.

De Ruig M.J. (1992) - *Tectono-sedimentary evolution of the Prebetic Fold Belt of Alicante (SE Spain).* Thesis Vrije University Amsterdam (Netherlands), 207 pp.

De Ruig M.J. (1995) - *Extensional diapirism in the eastern Prebetic foldbelt, south-eastern Spain.* In: M. P. A. Jackson, D.G. Roberts & S. Snelson (Eds.), Salt tectonics: a global perspective. A.A.P.G. Memoirs, **65**, 353-367.

Di Staso A., Perrotta S., Guerrera F., Perrone V. & Tramontana M. (2009) - *New biostratigraphic and petrographic data from the Poggio Carnaio Sandstone Fm (Val Marecchia Nappe): insights into the tectonic evolution of the Northern Apennines.* Italian Journal of Geosciences, **128**, 443-454.

Dorronsoro C. (1978) – *Contribution to the mineralogical study of the Subbetic Triassic*. Estudios Geológicos, **34**, 251-261.

Dou Y., Yang S., Liu Z., Clift P.D., Yu H., Berne S. & Shi X. (2010) - *Clay mineral evolution in the central Okinawa Trough since 28 ka: Implications for sediment provenance and paleoenvironmental change*. Palaeogeography, Palaeoclimatology, Palaeoecology, **288**, 108-117.

Drits V.A., Sakharov B.A., Lindgreen H. & Salyn A. (1997) - *Sequential structure transformation of illite-smectite-vermiculite during diagenesis of Upper Jurassic shales from the North Sea and Denmark*. Clay Minerals, **32**, 351-371.

Enu E.I. (1986) - *Influence of tectonics and palaeoenvironment on late Cretaceous clay sedimentation in the upper benue trough, Nigeria*. Geological Journal, **21**, 93-99.

Eslinger E, Mayer L, Durst T, Hower J. & Savin, S. (1973) - *A X-ray technique for distinguishing between detrital and secondary quartz in the fine grained fraction of sedimentary rocks.* Journal Sedimentary Petrology, **43**, 540-543.

Esquevin J. (1969) - *Influence de la composition chimique des illites sur la cristallinité.* Bulletin Centre Recherche. Pau, S.N.P.A., **3**, 147-154.

Estévez A., Martín-Rojas I., Alfaro P. & Martín-Martín M. (2007) - *The Ventós-Maigmó Strike-Slip Fault Zone (Alicante province, SE Spain): evidences of Miocene tectonic control on sedimentation.* Geophysical Research Abstracts, E.U.G., **9**, 1607-1609.

Gingele F.X., Müller P.M. & Schneider R.R. (1998) - *Orbital forcing of freshwater input in the Zaire Fan area – clay mineral evidence from the last 200 kyr.* Palaeogeography Palaeoclimatology Palaeoecology, **138**, 17-26.

Guerrera F., Martin-Algarra A. & Perrone V. (1993) - *Late Oligocene-Miocene syn- /-late-orogenic successions in Western and Central Mediterranean Chains from the Betic Cordillera to the Southern Apennines*. Terra Nova, **5**, 525-544.

Guerrera F., Martín-Martín M., Perrone V. & Tramontana M. (2005) - *Tectono-sedimentary evolution of the southern branch of the Western Tethys (Maghrebian Flysch Basin and Lucanian Ocean).* Terra Nova, **17**, 358-367.

Guerrera F., Estevez A., López-Arcos M., Martín-Martín M., Martín Pérez J.A. & Serrano F. (2006) - *Paleogene tectono-sedimentary evolution of the Alicante Trough (External Betic Zone, SE Spain) and its bearing on the timing of the deformation of the South-Iberian Margin.* Geodinamica Acta, **19**, 87-101.

Guerrera F., Mancheño M.A., Martín-Martín M., Raffaelli G., Rodríguez-Estrella T. & Serrano F. (2014) - *Paleogene evolution of the External Betic Zone and geodynamic implications*. Geologica Acta, **12**, 171-192.

Guerrera F. & Martín-Martín M. (2014) - *Paleogene-Aquitanian tectonic breakup in the eastern External Betic Zone (Alicante, SE Spain).* Rev. Soc. Geol. España, **27**, 271-285.

Handy M.R., Schmid S.M., Bousquet R., Kissling E. & Bernoulli D. (2010) - *Reconciling plate tectonic reconstructions of Alpine Tethys with geological-geophysical record of spreading and subduction in the Alps.* Earth-Sci. Reviews, **102**, 121-158.

Holtzapffel T. (1985) - *Les Minéraux Argileux: Préparation, Analyse Diffractométrique et Détermination*. Soc. Géol. Nord Publ., **12**, 136 pp.

Hunziker J.C. (1986) - *The evolution of illite to muscovite: an example of the behavior of isotopes in low grade metamorphic terrains*. Chem. Geol., **57**, 31-40.

Jamoussi F., Bédir M., Boukadi N., Kharbachi S., Zargouni F., López-Galindo A. & Paquet H. (2003) - *Répartition des minéraux argileux et contrôle tectono-eustatique dans les bassins de la marge tunisienne*. Compte Rendue de l'Académie des Science, Paris, **335**, 175-183.

Lanson B., Sakharov B.A., Claret F. & Drits V.A. (2009) - *Diagenetic smectite-to-illite transition in clay-rich sediments: a reappraisal of X-ray diffraction results using the multi-specimen method*. American Journal of Science, **309**, 476-516.

Liu Z., Tuo S., Colin C., Liu, J.T., Huang C.Y., Selvaraj K., Chen C.T.A., Zhao Y., Siringan F.P., Boulay S. & Chen Z. (2008) - *Detrital fine-grained sediment contribution from Taiwan to the northern South China Sea and its relation to regional ocean circulation.* Marine Geology, **255**, 149-155.

López-Galindo A. (1986) - *Mineralogía de series cretácicas de la Zona Subbética. Algunas consideraciones paleogeográficas derivadas de la composición química de las esmectitas.* Estudios Geológicos, **42**, 231-238.

López-Galindo A. & Oddone M. (1990) - *The distribution of clay minerals, rare-earths and trace elements in middle Cretaceous mudstones of the southern Iberian paleomargin*. Chemical Geology, **84**, 169-172.

López-Galindo A., Oloriz F. & Rodriguez-Tovar F. (1994) - *Geochemical traces and sequence stratigraphy analysis during the Upper Jurassic in Southern Iberia.* Mineralogical Magazine, **58/A**, 531-532.

Maaté S., Alcalá F.J., Guerrera F., Hlila R., Maaté A., Martín-Martín M., Raffaelli G., Serrano F. & Tramontana M. (2017) - *The External Tanger Unit (Intrarif sub-Domain, External Rifian Zones, Morocco): an interdisciplinary study.* Arabian Journal of Geosciences, **10**, 556. DOI: 10.1007/s12517-017-3347-8.

Martín-Martín M., Rey J., Alcalá F.J., Tosquella J., Deramond J., Lara-Corona E., Duranthon F. & Antoine P.O. (2001) - *Tectonic controls on the deposits of a foreland basin: an example from the Eocene Corbières-Minervois basin, France*. Basin Research, **13**, 419-433.

Martín-Martín M., Estévez A., Martín-Rojas I., Guerrera F. Alcalá F.J., Serrano F. & Tramontana M. (2017) - *The Agost Basin (Betic Cordillera, Alicante province, Spain): a pull-apart basin involving salt tectonics*. International Journal Earth Science (Geol. Rundsch), DOI 10.1007/s00531-017-1521-6

Martinez-Ruiz F., Ortega-Huertas M., Palomo I. & Barbieri M. (1992) - *The geochemistry and mineralogy of the Cretaceous-Tertiary boundary at Agost (southeast Spain)*. Chemical Geology, **95**, 265-281.

Mcdonnell A., Hudec M.R. & Jackson M.P.A. (2009) - *Distinguishing salt welds from shale detachments on the inner Texas shelf, western Gulf of Mexico*. Basin Research, **21**, 47–59.

Michard A., Chalouan H.A., Feinbergh H., Goffe B. & Montigny R. (2002) - *How does the Alpine belt end between Spain and Morocco?* Bulletin Société. Géologique de France, **173**, 3-15.

Moiroud A., Martinez M., Deconinck J.F., Monna F., Pellenard P., Riquier L., Company M. (2012) - *High-resolution clay mineralogy as a proxy for orbital tuning: Example of the Hauterivian-Barremian transition in the Betic Cordillera (SE Spain)*. Sedimentary Geology, **282**, 336-346.

Moore D.M. & Reynolds R.C. (1997) - *X-Ray Diffraction and the Identification and Analysis of Clay Minerals*. 2nd Ed. Oxford, New York: Oxford University Press, 378 pp.

Nadeau P.H. & Bain D.C. (1986) - *Composition of some smectites and diagenetic illitic clays and implications for their origin*. Clays and Clay Minerals, **34**, 455-464.

Palomo I., Ortega-Huertas M. & Fenoll-Hach-Alí P. (1985) - *The influence of clay minerals in studies of the evolution of the Jurassic deposits of the Betic Cordillera, SE Spain*. Clay Minerals, **20**, 39-52.

Perrone V., Perrotta S., Marsaglia K., Di Staso A. & Tiberi V. (2014) - *The Oligocene ophiolite-derived breccias and sandstones of the Val Marecchia nappe: Insights for paleogeogrphy and evolution of northern Apennines (Italy)*. Palaeogeography, Palaeoclimatology, Palaeoecology, **394**, 128-143.

Plestch T. (1997) - *Clay minerals in Cretaceous deep-water formations of the Rif and the Betic Cordillera*. Bulletin Société Géologique du Nord, **26**, 1-106.

Puy J.L. (1979) - *Mineralogía y geoquímica del Trías de la Zona Subbética de Huelma (Jaén)*. PhD Thesis, Univ. Granada, Spain, 531 pp.

Righi D. & Elsass F. (1996) - *Characterization of soil clay minerals; decomposition of X-ray diffraction diagrams and high-resolution electron microscopy*. Clays and Clay Minerals, **44**, 791-800.

Ruffell A.H., Price G.D., Mutterlose J., Kessels K., Baraboshkin E. & Gröcke D.R. (2002) - *Palaeoclimate indicators (clay minerals, calcareous nannofossils, stable isotopes) compared from two successions in the late Jurassic of the Volga Basin (SE Russia)*. Geological Journal, **37**, 17-33.

Sanz De Galdeano, C. & Vera J.A. (1992) - *Stratigraphic record and paleogeographical context of the Neogene basins in the Betic Cordillera, Spain*. Basin Research, **4**, 21-36.

Sanz De Galdeano C. & Buforn E. (2005) - *From strike-slip to reverse reactivation: The Crevillente Fault System and seismicity in the Bullas-Mula area (Betic Cordillera, SE Spain)*. Geologica Acta, **3**, 241-250.

Schultz L.G. (1964) - *Quantitative interpretation of mineralogical composition from x-ray and chemical data for the Pierre Shale*. U.S. Geol. Survey Professional Paper 391-C, 31 pp.

Sissingh W. (2008) - *Punctuated Neogene tectonics and stratigraphy of the African-Iberian plate boundary zone: concurrent development of Betic-Rif basins (southern Spain, northern Morocco)*. Netherlands Journal of Geosciences, **87**, 241-289.

Tent-Manclús J.E., Estévez A. & Martín-Martín M. (2000) - *Olistrostromas originados por laciares de sal al Sur de la Sierra del Cajar (Cuenca neógena de Mula, Murcia)*. Geotemas, **1**, 273-276.

Twiss R.J. & Moores E.M. (2007) - *Structural Geology*. 2nd ed., Freeman Ed., New York, 736 pp.

Vera J.A. (2000) - *El Terciario de la Cordillera Bética: estado actual de conocimientos*. Revista de la Sociedad Geológica de España, **12**, 345-373.

Vera J.A. (2004) - *Geología de España*. *IGME* – Sociedad Geológica España, 884 pp.

Wenkert D.D. (1979) - *The flow of salt glacier*. Geophysical Research Letters, **6**, 553-556.

Manuscript received 30 November 2017; accepted 10 April 2018; published online 13 March 2018;
editorial responsibility and handling by D. Cosentino